ORIGINAL RESEARCH ARTICLE

Using high-resolution XRF analyses as a sequence stratigraphic tool in a mudstone-dominated succession (Early Cretaceous, Lower Saxony Basin, Northern Germany)

Hauke Thöle[1,2] | André Bornemann[2] (ID) | Ulrich Heimhofer[1] | Friedrich Wilhelm Luppold[3] | Martin Blumenberg[2] | Reiner Dohrmann[2,3] | Jochen Erbacher[2,3]

[1]Institute for Geology, Leibniz University Hannover, Hannover, Germany

[2]Federal Institute for Geosciences and Natural Resources (BGR), Hannover, Germany

[3]State Authority for Mining, Energy and Geology (LBEG), Hannover, Germany

Correspondence
Hauke Thöle, Federal Institute for Geosciences and Natural Resources (BGR), Hannover, Germany.
Email: hauke.thoele@bgr.de

Funding information
Federal Institute for Geosciences and Natural Resources (BGR)

Abstract

Delineation of stratigraphic sequences and their component systems tracts in mudstone-dominated successions is challenging due to the relatively homogenous, fine-grained nature of the strata. High-resolution elemental intensity data from X-ray fluorescence core scanning is used in order to develop a sequence stratigraphic framework for the Lower Cretaceous monotonous mudstone succession in the eastern Lower Saxony Basin. The study is based on four drill cores covering the Berriasian to Aptian interval. In addition, carbon isotope ($\delta^{13}C_{org}$), grain size and $CaCO_3$ analyses were carried out on discrete samples. The studied cores represent both proximal and distal basinal environments of the eastern Lower Saxony Basin and can be reliably correlated by utilizing variations in selected X-ray flourescence elemental ratios, K/Ti data have proven to be particularly suitable in this regard. The core correlation shows that chemostratigraphic variability within the studied succession is laterally reproducible in the eastern Lower Saxony Basin, and can be used to establish a sequence stratigraphic framework. Further, Si/Al and Ca/Ti ratios have been applied to characterize the cores in terms of variation in grain size and $CaCO_3$ content, respectively. Vertical grading trends inferred from Si/Al changes were used to identify transgressive and regressive systems tracts within the studied succession. An important regression in the uppermost lower Valanginian coincides with the onset of the Valanginian Weissert Event, as indicated by the well-known positive $\delta^{13}C$ shift, and, thus, supports the idea that the initial interval of this event corresponds to enhanced supply of terrigenous material. The results of this study are also in agreement with previously recognized transgressive–regressive trends in the Lower Saxony Basin and adjacent areas. This clearly shows that systematic geochemical variations recorded in mudstone-dominated basinal settings are suitable to establish sequence stratigraphic frameworks.

KEYWORDS
Lower Cretaceous, Lower Saxony Basin, mudstones, sequence stratigraphy, Weissert Event, X-ray fluorescence core scanning

1 | INTRODUCTION

Mudstones are the most common sedimentary rocks (Picard, 1971; Wedepohl, 1971; Stow, 1981) and some of the most challenging to study, analyse and understand. Despite having a homogeneous appearance on a macroscopic scale, mudstones (rocks predominately composed of sedimentary materials <62.5 μm; Lazar *et al.*, 2015) are typically highly heterogeneous in terms of composition and texture, and often formed via a range of depositional processes (Macquaker *et al.*, 2007; Abouelresh and Slatt, 2011, 2012; Aplin and Macquaker, 2011; Hammes *et al.*, 2011; Hammes and Frébourg, 2012). Because mudstone-dominated sedimentary successions are being increasingly targeted as unconventional hydrocarbon reservoirs and as host rocks for geological disposal, there has been a significant advance in our understanding of the sedimentology and stratigraphy of mudstones over the last decade, especially concerning the pervasive facies variability present within these fine-grained rocks (Bohacs and Schwalbach, 1992; Macquaker *et al.*, 2007; Macquaker *et al.*, 2010; Hammes *et al.*, 2011; Abouelresh and Slatt, 2012).

Sequence stratigraphic methodologies are now being used more commonly to interpret apparently homogeneous, fine-grained clastic successions, since it has been recognized that variability is often systematic and can be interpreted in terms of varying detrital inputs, biological productivity and subsequent diagenesis using sequence stratigraphic principles (Bohacs and Schwalbach, 1992; Schwalbach *et al.*, 1992; Macquaker and Taylor, 1996; Macquaker *et al.*, 1998; Macquaker *et al.*, 2007; Singh, 2008). Delineation of stratigraphic sequences and their component systems tracts in such fine-grained sedimentary rocks, however, is challenging, and it is certainly not as straightforward as in coarse-grained sedimentary systems (Ver Straeten *et al.*, 2011). The apparent macroscopic-scale homogeneity that dominates most mudstone-dominated sedimentary successions makes a reliable determination of transgressive-regressive facies cycles based on visual inspection alone quite challenging and time consuming. An approach that has recently been used to establish sequence stratigraphic frameworks in mudstone-dominated basinal settings without clear ties to coastal records, is to determine systematic stratigraphic variations in the inorganic and organic geochemistry of sedimentary rocks (Ver Straeten *et al.*, 2011; Turner *et al.*, 2015, 2016). These variations are subsequently used to characterize and define stratigraphic sequences. Such approaches rely upon the fact that even apparently homogeneous mudstones show changes in their chemical composition.

Geochemical analysis by X-ray fluorescence (XRF) core scanning (CS) has become a well-accepted and intensively used analytical method to investigate the elemental composition of marine and terrestrial sediments (Rothwell and Rack, 2006). The rapid and non-destructive analytical capability of XRF core scanners allows the acquisition of high-resolution geochemical data sets in a relatively short time.

Here, this method is used to analyse four sediment cores from Northern Germany in order to discern the geochemical variability present within the mudstone-dominated Lower Cretaceous succession in the eastern Lower Saxony Basin (LSB; Figure 1A). The four drill sites cover the time interval from the latest Berriasian to earliest Aptian (Figure 1C). This study aims at developing a sequence stratigraphic framework for the Lower Cretaceous succession in the eastern LSB, and associating facies variability of the studied sediments with sequences and systems tracts. To date, only a few sequence stratigraphic interpretations of shallow marine, proximal formations that served as regionally important petroleum reservoirs in the past are available for the LSB. These include the lower Valanginian Bentheim Formation at the western margin of the LSB (Wonham *et al.*, 1997; Stadtler, 1998). A correlation to distal successions is still lacking. A more comprehensive overview of transgressive-regressive cycles in the LSB during the Lower Cretaceous is given by Mutterlose and Bornemann (2000), albeit lacking a sequence stratigraphic interpretation. The nearly continuous nature of the cored succession, spanning the uppermost Berriasian to lower Aptian, offers an outstanding opportunity for testing the potential of XRF CS as a tool for sequence stratigraphy and establishing a more comprehensive sequence stratigraphic framework for the LSB.

2 | GEOLOGICAL SETTING AND PALAEOGEOGRAPHIC SITUATION

The studied boreholes are situated in the central to eastern part of the LSB (Figure 1B). The LSB is one of several Late Jurassic–Early Cretaceous rift and wrench induced basins in Western Europe and is bordered by the London-Brabant, Rhenish and Bohemian massifs (Betz *et al.*, 1987). During the Early Cretaceous, the LSB is situated north of the Rhenish Massif and extends from the East Netherlands High in the west to the Gifhorn Trough in the east. In the north, the connection to the proto North Sea was initially restricted by the Pompeck´ Swell (Figure 1B). These borders form a WNW–ESE trending intracontinental basin, approximately 280 km long and 80 km wide (Mutterlose and Bornemann, 2000). The LSB was episodically connected to the Tethys via the Carpathian seaway and the Paris Basin due to episodically occurring transgressions (Mutterlose, 1992; Mutterlose and Böckel, 1998) (Figure 1A). Marked subsidence of the LSB began during the Late Jurassic and continued into the early Late Cretaceous, when it was terminated by basin inversion (Betz *et al.*, 1987).
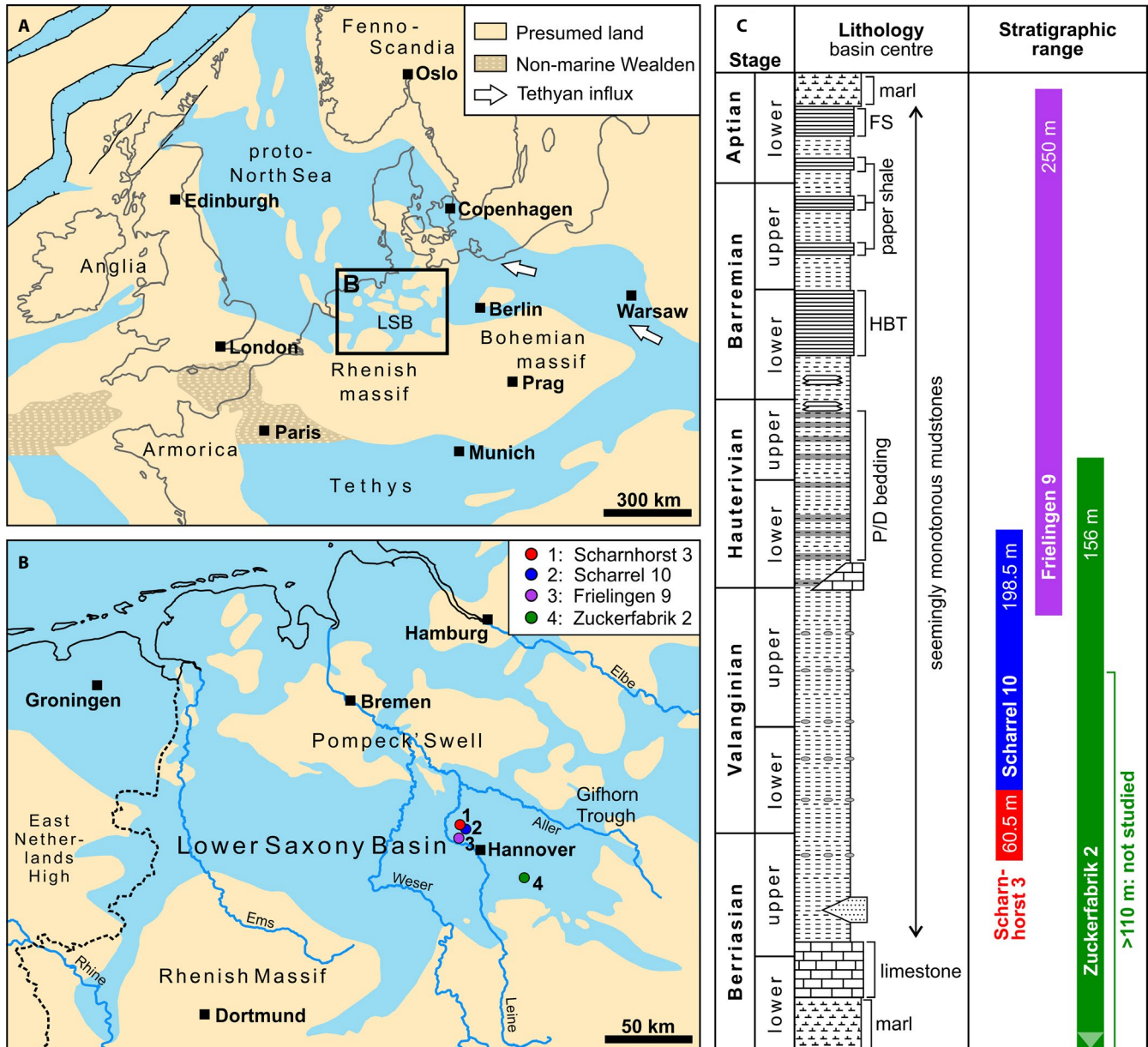
FIGURE 1 (A) Palaeogeographic map for the Valanginian/Hauterivian of NW Europe (adopted from Mutterlose, 1992). (B) Palaeogeographic map of the Lower Saxony Basin (LSB) during Hauterivian times (after Schott et al., 1967/1969) with the location of studied drill cores (Scharnhorst 3, Scharrel 10, Frielingen 9 and Zuckerfabrik 2). (C) Lithostratigraphy of the Early Cretaceous succession (Berriasian–lower Aptian) in the eastern central LSB (modified after Mutterlose and Bornemann, 2000) and stratigraphic ranges of studied cores

More than 2,000 m of Lower Cretaceous sediments (Berriasian–Albian) were accumulated in the subsiding LSB (Mutterlose and Bornemann, 2000). Along the basin margins, coarse-grained clastics were deposited throughout Valanginian to Aptian times. Towards the central parts of the basin, these coarse clastics are replaced by finer grained siliciclastics. Sediments of the basin centre are lithologically characterized by dark grey-coloured clay-rich mudstones that are poor in calcium carbonate ($CaCO_3$) and contain sideritic nodules. Pale-dark bedding rhythms on a scale of 0.5–1 m are common in the upper Hauterivian to Barremian (Figure 1C). These colour variations are mainly related to varying $CaCO_3$ content and are commonly explained by climate cycles within the Milankovitch frequency band (Mutterlose and Ruffell, 1999). Intercalated within these homogenous mudstones, some finely laminated horizons occur in the Barremian to lower Aptian succession (Figure 1C). These so-called paper shales (Blättertone) are rich in both organic matter and $CaCO_3$ and were accumulated under anoxic bottom water conditions (Mutterlose *et al.*, 2009). A distinctive paper shale horizon, the so-called Hauptblätterton, is developed in the lower Barremian (Figure 1C). Another finely laminated horizon, known as the Fischschiefer, represents the local

expression of the Early Aptian Oceanic Anoxic Event 1a (OAE1a). The Fischschiefer is overlain by pale marls, which indicate a change in the depositional environment towards hemipelagic conditions (Mutterlose *et al.*, 2009). More detailed descriptions of the evolution of the basin have been given by Schott *et al.* (1967/1969), Michael (1974, 1979), Kemper (1979), Betz *et al.* (1987), Mutterlose (1992) and Mutterlose and Bornemann (2000).

3 | MATERIAL AND METHODS

The present study focusses on four sediment cores from Northern Germany: Scharnhorst 3, Scharrel 10, Frielingen 9 and Zuckerfabrik 2 (Figure 1B). These cores were drilled between 2012 and 2016 by the State Authority for Mining, Energy and Geology (LBEG) and the Federal Institute for Geosciences and Natural Resources (BGR) in order to recover an expanded succession of Lower Cretaceous sediments within the LSB. The drill sites of Scharnhorst 3 and Scharrel 10 are located about 22 km northwest of Hannover, close to the village of Scharrel, and are situated ~2 km apart (Scharnhorst 3:52°31′48″N/9°32′30″E; Scharrel 10:52°31′21″N/9°34′22″E). The Frielingen 9 core has been drilled adjacent to the village of Frielingen, about 17 km northwest of Hannover (52°27′21″N/9°32′1″E). The fourth core, named Zuckerfabrik 2, was drilled about 35 km southeast of Hannover, close to the village of Hoheneggelsen (52°13′28″N/10°11′39″E).

All four cores have been studied using XRF CS, grain size analyses and sedimentary geochemistry ($CaCO_3$, total organic carbon [C_{org}] and $δ^{13}C_{org}$). In addition, the entire core was visually described and biostratigraphic analyses of calcareous nannofossils, benthic foraminifera and ostracods were conducted to constrain the age of the studied sections. All cores are curated at the BGR core repository in Berlin-Spandau.

3.1 | XRF core scanning

Macroscopic-scale homogeneity of the Lower Cretaceous mudstones recovered at the drill sites hampers the visual identification of transgressive-regressive facies cycles, however, cyclic changes may be apparent in the chemical composition of the sediments. To detect these, the entire core was scanned with an Avaatech XRF Core Scanner housed at the BGR core repository in Berlin-Spandau. The XRF CS measurements were obtained directly at the split core surface of the archive half of each core. Prior to the measurement, the sediment surface was lightly scraped with glass slides or metal scrapers to minimize surficial micro-relief and to remove any contamination of the core surface. After that, the surface was covered with a 4 μm thick SPEXCerti Prep Ultralene® foil to avoid contamination of the XRF measurement unit and desiccation of the

sediment. All XRF-CS measurements were conducted with a 10 keV setting, a current of 0.5 mA, no filter and a sampling time of 10 s to obtain the element intensities from Aluminium (Al) through iron (Fe). Measuring step size was 1 cm, with an irradiated sample surface of 1 cm^2. After CS was completed, the XRF spectral data were converted to a record of net element intensities (expressed as counts per unit time per unit area) using the iterative least square software package (WIN AXIL, Canberra Eurisys). In order to minimize the impact of measurement noise on succeeding analyses, XRF-CS data quality were cleaned using standard procedures (for details see Tjallingii, 2007). The filtered core scanner data were subsequently converted into additive log-ratios (alr) of element intensities as these provide the most robust record of relative chemical changes and lessen interpretation uncertainties (Weltje and Tjallingii, 2008). The calculation of log-ratios follows the concept of Aitchison (1986) for compositional data, and was performed using the R 'compositions' package (van den Boogaart and Tolosana-Delgado, 2008).

Both core preparation and subsequent verification of XRF-CS data can be time-consuming, especially when mudstones are altered after prolonged storage periods, as was the case for the Scharnhorst 3 and Scharrel 10 cores. These cores were sawed some time prior to XRF-CS with the result that most split cores were already noticeably altered, evidenced by prolific gypsum crystal blooms at the core surface and partly by extensive flaking and cracking of the dried-out sediment. Cleaning of the core surfaces is an important prerequisite for reliable XRF measurements and was relatively time-consuming. Despite careful cleaning, the acquired XRF-CS data of the altered cores revealed a number of erroneous XRF-CS measurements, which were characterized by extremely low Al intensities, accompanied by conspicuous high Ca readings. High Ca counts are likely attributed to gypsum at the core surface. In order to minimize these problems, it is recommended that cores are measured right after core splitting as was done for the Frielingen 9 and Zuckerfabrik 2 cores.

3.2 | Conventional XRF analyses

A total of 556 powdered samples (Frielingen 9: $n = 219$; Scharrel 10: $n = 193$; Scharnhorst 3: $n = 45$, Zuckerfabrik 2: $n = 99$) were analyzed for major and trace elements using a PANalytical Axios spectrometer (ALMELO). Samples were prepared by mixing with a flux material (lithium metaborate Spectroflux, flux no. 100A, Alfa Aesar) and melting into glass beads. The beads were analyzed by wavelength-dispersive XRF. To determine loss on ignition, 1,000 mg of the sample material was heated to 1,030°C for 10 min. The calibrations are validated by analyses of reference materials. 'Monitor' samples and 130 certified reference materials are used for correction procedures.

3.3 | Grain size analyses

Grain size analyses (Frielingen: $n = 218$; Scharrel 10: $n = 193$; Scharnhorst 3: $n = 45$; Zuckerfabrik 2: $n = 99$) were used to test whether geochemical variation determined by XRF-CS measurement mirror textural parameters in the studied cores. The grain size distribution was determined through a combined sieving (particles >63–2,000 μm) and sedimentation (particles <63 μm) investigation in support of DIN ISO 11277 (compare Müller *et al.*, 2009). Ten grams of each sample were dispersed in deionized water and homogenized two times for 20 s each by ultrasonic treatment. The fraction <63 and >63 μm were separated by wet sieving and recovered by lyophilization. The fractions >63 μm were then separated by ordinary dry sieving using a CAMSIZER® dynamic image analysis system (Retsch Technology). After dispersion using 0.01 n tetra-sodiumdiphosphate decahydrate the fractions <63 μm were analyzed using a MICROMETRICS SediGraph 5100™ Particle Size Analysis System at the BGR. Grain size measurements were validated by analysis of reference material. For quality control of all 10 measured grain size fractions an internal standard material was added to each series of 17 samples.

3.4 | CaCO$_3$ and C$_{org}$ analyses

In order to estimate the CaCO$_3$ content continuously throughout the studied interval, a set of discrete CaCO$_3$ measurements were used to calibrate a high-resolution XRF-estimated CaCO$_3$ profile as applied in other studies (Bornemann *et al.*, 2017; Salabarnada *et al.*, 2018). Total carbon (TC) and C$_{org}$ were measured on 910 samples (Frielingen: $n = 427$; Scharrel 10: $n = 230$; Scharnhorst 3: $n = 52$; Zuckerfabrik 2: $n = 201$) using a LECO CS230 carbon–sulphur analyser at the BGR. The CaCO$_3$ contents (wt%) were calculated using a standard equation based on molecular weights: CaCO$_3$ = [TC−C$_{org}$] × 8.33. The best correlation between wt% CaCO$_3$ and XRF-CS measurements was obtained applying a 10-point moving average to alr(Ca/Ti). The Ca/Ti ratios were calibrated to CaCO$_3$ concentrations (wt%) by applying a regression equation that was derived from a third-order polynomial correlation ($R^2 = 0.75$) of scanner measurements and conventional CaCO$_3$ data. Similar correlation coefficients were found for centred log ratios (clr) of Ca (polynomial: $R^2 = 0.72$). Due to their good correlation with conventional CaCO$_3$ measurements, both ratios seem to be capable of highlighting variations in the CaCO$_3$ content. Because of the slightly better correlation, the alr(Ca/Ti) is used as a proxy for CaCO$_3$ content in this study, 'CaCO$_3$ *est.*' is used throughout the text to refer to carbonate content estimated by alr(Ca/Ti).

3.5 | δ^{13}C$_{org}$ analyses

Carbon isotope analyses of bulk organic matter (δ^{13}C$_{org}$) were carried out on 556 samples (Scharnhorst 3: $n = 55$; Scharrel 10: $n = 293$; Frielingen 9: $n = 208$, Zuckerfabrik 2: $n = 102$). Most of these samples ($n = 532$) were measured after decalcification with HCl at the BGR, using a Thermo Flash EA 1112 elemental analyzer coupled via a Conflo IV interface to an Isotope Ratio Mass Spectrometer (Thermo Delta V Advantage). A Thermo Scientific Flash 2000 organic element analyser connected to a Thermo Delta V Advantage Isotope Ratio Mass Spectrometer, available at the Institute for Geology, Leibniz University Hannover, has been used to analyse a set of samples from the Scharrel 10 core ($n = 126$). All stable isotope results are given in δ-notation with respect to the V-PDB standard and had a reproducibility of <0.2‰.

4 | AGE CONTROL AND CHEMOSTRATIGRAPHIC CORRELATION

A detailed core-to-core correlation among sites was achieved by integrating XRF-CS elemental data with isotope and biostratigraphy. The chronostratigraphic framework has primarily been constrained by calcareous nannofossil biostratigraphy following Bown *et al.* (1998). Additional stratigraphic control is provided by δ^{13}C chemostratigraphy and for the Berrriasian to Valanginian interval by regional biostratigraphy based on benthic foraminifera and ostracods (Bartenstein and Brand, 1951; Wolburg, 1959; Bartenstein and Bettenstaedt, 1962; Figure 2). The results suggest a late Berriasian to early Valanginian age for the 60.5 m long Scharnhorst 3 core, which was drilled as a downward continuation of the 198.5 m long Scharrel 10 core. Sediments of the Scharrel 10 core have been stratigraphically assigned to the upper lower Valanginian to lower Hauterivian (Boreal nannofossil Biozones BC4–BC7). The Frielingen 9 core is 250 m long and covers the time interval from the late Valanginian to the early Aptian (BC5-BC19/20 Biozones), whereby the short duration of certain nannofossil zones may indicate some degree of stratigraphic condensation, or more likely the lack of stratigraphic marker species in the LSB. The 156 m long Zuckerfabrik 2 core covers the time interval from the Oxfordian to the upper Hauterivian. This study focuses on the ~102 m thick (depth interval: 8–110 m) upper Valanginian to lowermost upper Hauterivian mudstone succession (BC5–BC9).

Variations and trends in selected XRF elemental ratios in combination with the established chronostratigraphic framework allowed a precise chemostratigraphic correlation among sites. The elemental K/Ti ratio has been used in other studies as an indicator of weathering and erosion intensity (Muhs *et al.*, 2001; Piva *et al.*, 2008; Arnaud *et al.*, 2012; Matys Grygar *et al.*, 2017, 2019) or for provenance
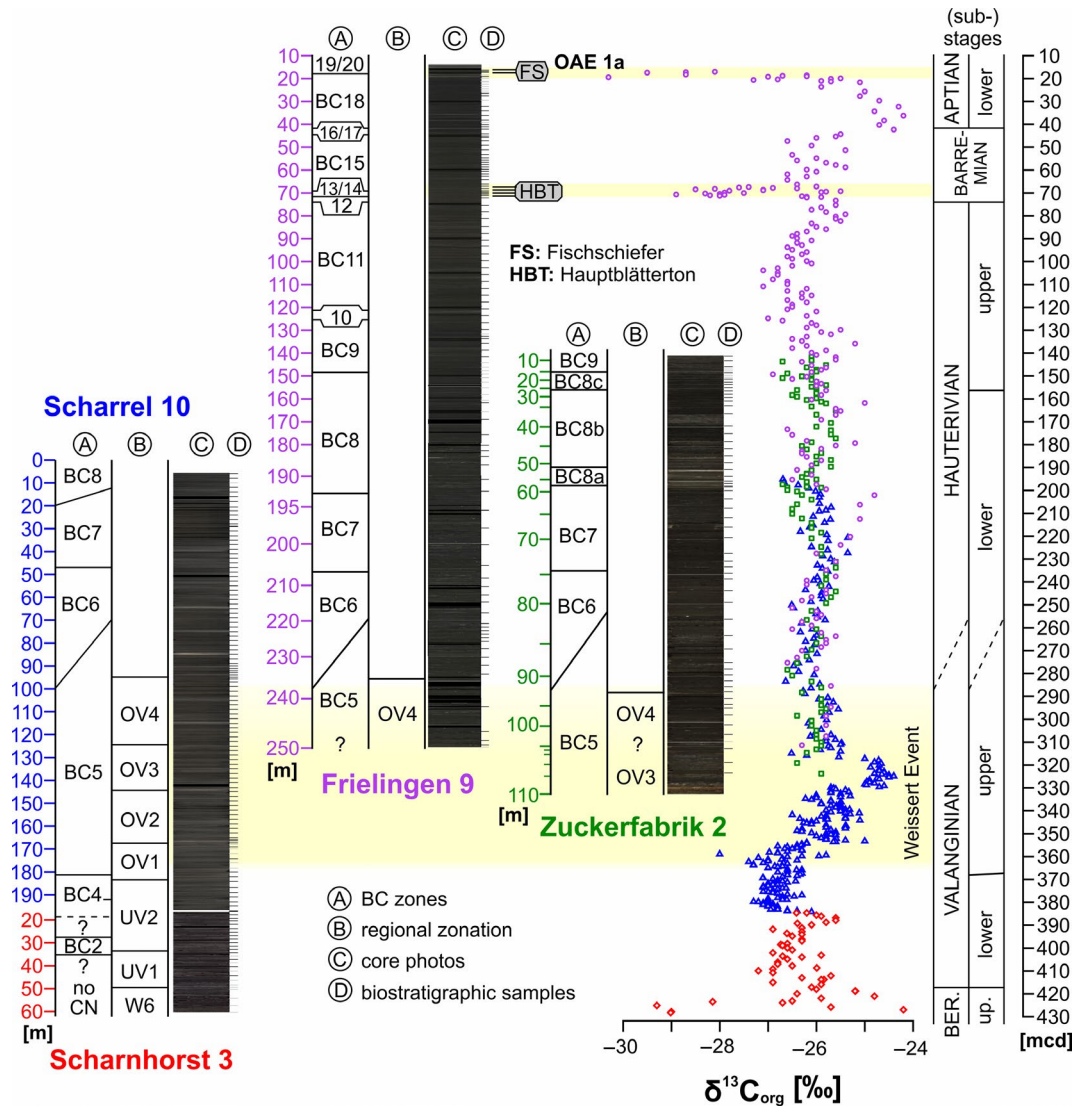
FIGURE 2 Biostratigraphy, chemostratigraphy ($\delta^{13}C_{org}$) and key events covered by the studied cores. A combination of $\delta^{13}C$ chemostratigraphy and calcareous nannofossil biostratigraphy was used to establish the chronostratigraphic framework. A regional stratigraphic zonation scheme based on benthic foraminifera and ostracods is additionally provided. A composite depth scale (referred to as metres composite depth; mcd) was constructed using the depth scale of core Frielingen 9 for the upper 186.7 m, for the middle part the entire depth scale of Scharrel 10, and the part below 17 m in core Scharnhorst 3 for the lowermost interval. BC zones, Boreal calcareous nannofossil zones; OAE, oceanic anoxic event

analyses (Diekmann *et al.*, 2008; Kujau *et al.*, 2010; Monien *et al.*, 2012) and has proved to be particularly suitable in this regard. In the herein studied sediments K is predominantly built into illitic phyllosilicates/micas and in K-bearing feldspar. Potassium is easily leached by weathering processes, whereas Ti is considered rather stable, thus weathering in the hinterland might be an important factor controlling K/Ti. Since the study area of the LSB is relatively small it is likely that the observed changes occur synchronous among the studied sites (Matys Grygar *et al.*, 2017). The overlapping intervals of the studied cores show similar K/Ti variations and trends and a marked triple peak in the K/Ti profiles situated slightly above the Valanginian–Hauterivian boundary provides an unequivocal tie point for

correlation. Additional tie points were set based on distinct peaks and troughs in the K/Ti curves as well as based on marked features in the Ca/Ti trends (Figure 3). The Ca/Ti ratios which were calibrated to $CaCO_3$ concentrations (wt%) are also rather congruent throughout the overlapping intervals, but generally less useful for correlation than the K/Ti data. The Ca/Ti ratios do not allow for a proper correlation among sites, but are suitable to refine core correlations depicted by the K/Ti trends.

The overall trend observed in the composite $\delta^{13}C_{org}$ record for the studied succession (Figure 2) is in good accordance with existing Lower Cretaceous carbon isotope curves and enables the identification of characteristic chemostratigraphic events. The carbon isotope record of the Lower Cretaceous is
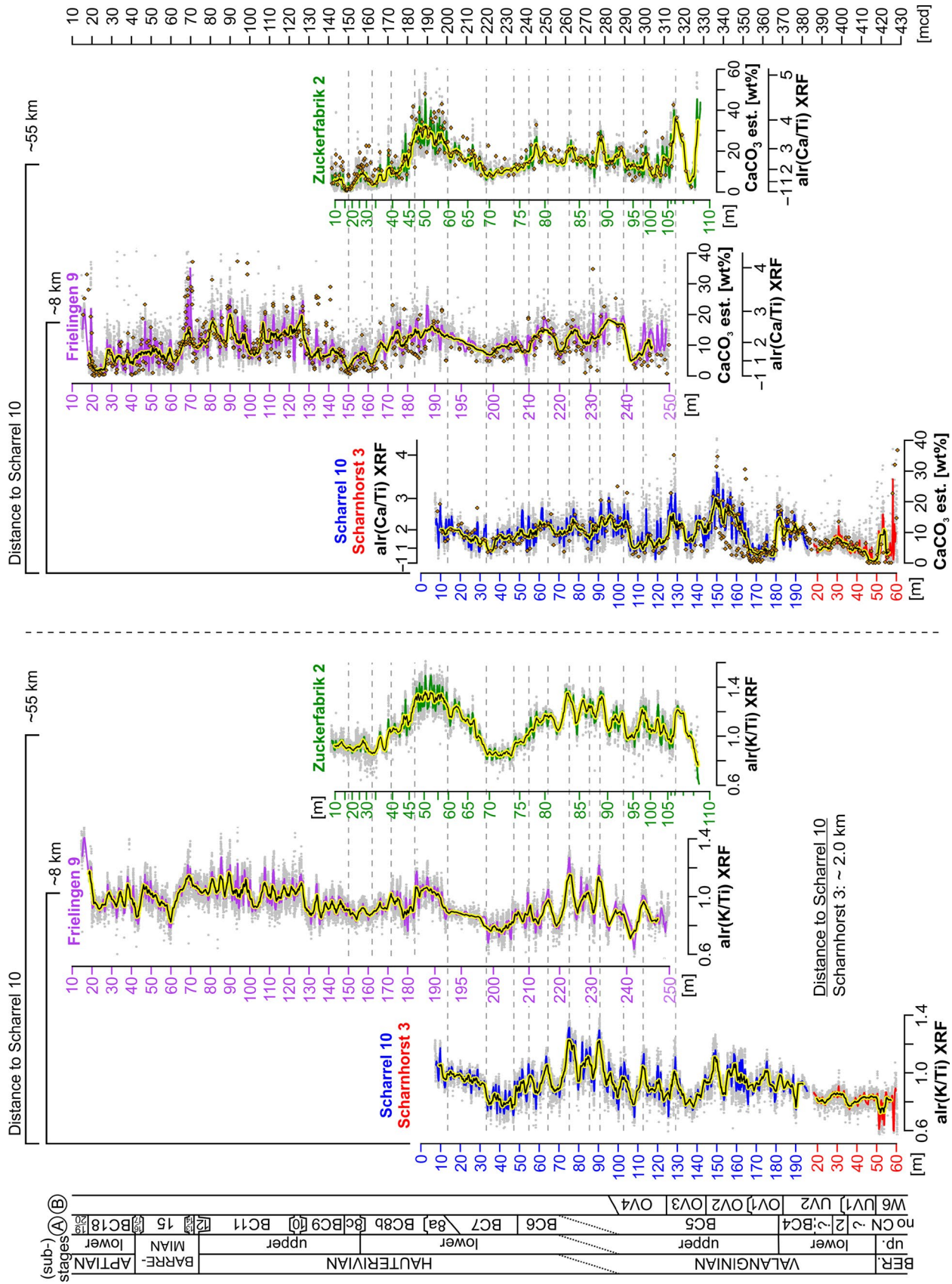
FIGURE 3 Detailed core-to-core correlation among sites based on XRF elemental ratios (K/Ti and Ca/Ti) and biostratigraphic information. (A) Boreal calcareous nannofossil zones and (B) regional zones based on benthic foraminifera and ostracods. CaCO$_3$ est.: additive log ratios (alr) of Ca/Ti XRF core scanning data have been numerically calibrated to discrete CaCO$_3$ measurements (orange dots). For XRF data, the yellow-black lines represent a 5 m moving-average (MA) and other coloured lines (red, blue, purple and green) a 0.5-m MA

marked by several excursions related to perturbations of the global carbon cycle (Weissert *et al.*, 1998). Further, the apparently synchronous variations in $\delta^{13}C_{org}$ values in the overlapping core intervals further confirm the established core correlations (Figure 2) based on XRF-CS.

The $\delta^{13}C_{org}$ signals vary between −30.3 and −24.2‰. Three distinct carbon isotope excursions (CIEs) are observed in the studied succession. These include a marked positive CIE, which starts at the lower Valanginian – upper Valanginian transition. The CIE reaches its maximum in the middle upper Valanginian, and returns in the uppermost Valanginian to values that are slightly more positive than prior to the excursion (Figure 2). This well-defined positive $\delta^{13}C_{org}$ anomaly can be stratigraphically correlated to the global Weissert Event (Erba *et al.*, 2004), and is herein documented for the first time in the LSB. This CIE is associated with a globally recorded positive $\delta^{13}C$ excursion in carbonate ($\delta^{13}C_{carb}$), and in organic material ($\delta^{13}C_{org}$) of marine and terrestrial origin (Lini *et al.*, 1992; Wortmann and Weissert, 2000; Gröcke *et al.*, 2005; Bornemann and Mutterlose, 2008) and co-occurs with a pulse in volcanic activity and the formation of the Paraná-Etendeka large igneous province, enhanced pCO_2 input in the ocean-atmosphere system, and greenhouse-like conditions (Lini *et al.*, 1992; Föllmi *et al.*, 1994; Weissert *et al.*, 1998; Martinez *et al.*, 2015).

Beside the Weissert Event, two distinct negative shifts in $\delta^{13}C_{org}$ are recorded in the lower Barremian and lower Aptian, respectively (Figure 2). The first negative CIE occurs in the lower Barremian (Biozones BC13/14 to lower BC15), with $\delta^{13}C_{org}$ values as low as −28.9‰ and corresponds to a distinct paper shale horizon with high C_{org} and $CaCO_3$ contents, known as the Hauptblätterton. Negative $\delta^{13}C$ values have previously been documented for the lower Barremian Hauptblätterton and are interpreted to reflect a regional or diagenetic signal in the semi-restricted LSB (Mutterlose *et al.*, 2009; Pauly *et al.*, 2013). A further prominent negative CIE is developed in the lower Aptian Fischschiefer (uppermost BC18–BC19/20), reaching $\delta^{13}C_{org}$ values as low as −30.3‰ (Figure 2). This paper shale horizon is often interpreted as local expression of the global OAE 1a (Bottini and Mutterlose, 2012; Heldt *et al.*, 2012), which is characterized by widespread deposition of organic-rich shales. The globally observed OAE 1a shows a pronounced negative $\delta^{13}C$ shift at its base; followed by a large positive excursion (Menegatti *et al.*, 1998).

5 | RESULTS

5.1 | Lithological characteristics

5.1.1 | Composite section (distal basinal setting)

Because of their close vicinity and similar geochemical signatures, the Scharnhorst 3, Scharrel 10 and Frielingen 9 cores

were considered as one complete ~430 m thick composite section, spanning the upper Berriasian to lower Aptian (Figures 3 and 4). The recovered sediments were accumulated in a distal basinal setting (Figure 1B) and consist of predominately rather monotonous dark grey-coloured fine mudstones. Clay (<2 μm) and very fine silt (2–6.3 μm) is the dominant fraction in most of the analysed grain size samples, with an average content of 77 wt% (Figure 4). Coarser grained sediments are recognized in the uppermost Berriasian, around the lower Valanginian–upper Valanginian boundary, as well as in the lower Aptian.

The $CaCO_3$ est. content is highly variable, ranging from less than 1 wt% to more than 40 wt%, with an average around 10 wt% (Figures 3 and 4). A few moderately to densely packed shelly laminae are observed in the Berriasian part of the Scharnhorst 3 core. Moreover, a 10 cm thick interval at the base of the core contains shale rip-up clasts. Distinct pale-dark bedding rhythms are developed in the middle lower Hauterivian and in the upper Hauterivian. The pale beds show thicknesses of about 0.3–1 m and are generally characterized by relatively high $CaCO_3$ est. contents compared to the adjacent dark layers. The dark beds are generally thicker and visually less bioturbated than the lighter intervals, which often show distinctive bioturbation patterns.

The C_{org} content of the mudstones varies between 0.2 and 7.3 wt%. The highest C_{org} values are recognized throughout the Barremian to lower Aptian interval and are commonly restricted to the occurrence of finely laminated, $CaCO_3$-rich horizons (Figure 4). The most prominent of these laminated horizons is the Hauptblätterton in the lower Barremian. Another distinct finely laminated horizon, known as Fischschiefer, occurs in the lower Aptian. Pyrite in the form of scattered crystals, small nodules and tiny lenses is quite common throughout the composite section, particularly in the uppermost Hauterivian to lower Aptian interval (Figure 4). Furthermore, sideritic and calcareous concretions are present at several levels within the rather monotonous dark grey-coloured fine mudstones.

5.1.2 | Zuckerfabrik 2 (proximal basinal setting)

The Zuckerfabrik 2 core represents a section deposited in a more proximal portion of the basin as compared to the distal composite section (Figure 1B). The stratigraphic overlap between the composite record and the Zuckerfabrik 2 core covers the middle upper Valanginian to lowermost upper Hauterivian (131 metres composite depth [mcd] to 331 mcd). The lowermost Valanginian sediments recovered from the Zuckerfabrik 2 core (depth interval: >109 m) consist of medium to coarse-grained, moderately to poorly sorted, partly unconsolidated sands
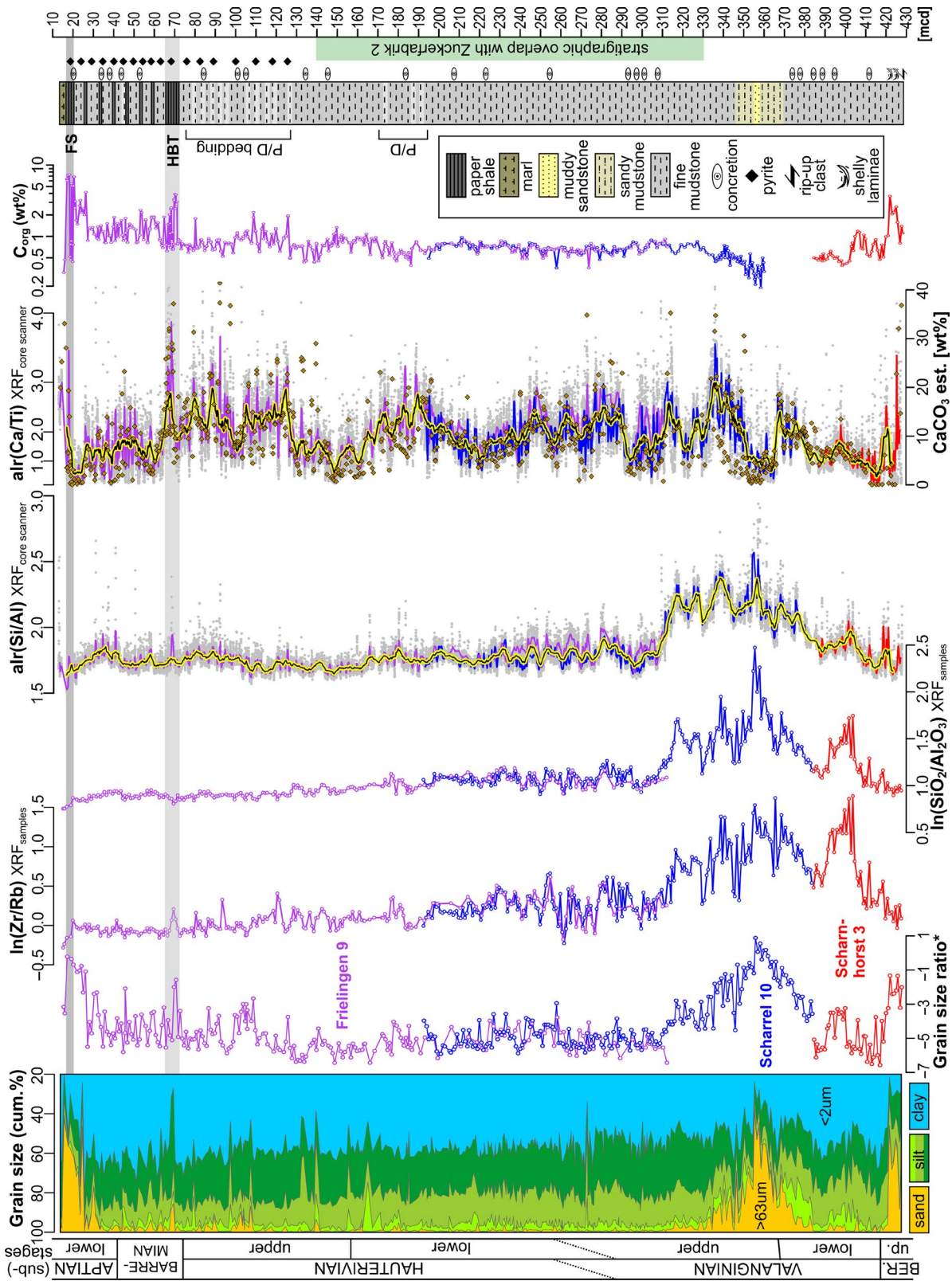
FIGURE 4   Composite record of the drill cores Scharnhorst 3, Scharrel 10 and Frielingen 9 showing grain size data, Si/Al and Ca/Ti ratios obtained by XRF core scanning, Zr/Rb and SiO₂/Al₂O₃, based on conventional XRF measurements, C_org content, and the lithological log. Grain size data are presented as both cumulative weight percentages (sand >63 μm; coarse silt: 20–63 μm; medium silt: 6.3–20 μm; fine silt: 2–6.3 μm; clay: <2 μm), and as log ratios of a coarse fraction (63 and 630 μm, fine to medium sand) to a fine fraction (<63 μm, clay to coarse silt). The log ratios of Zr/Rb and Si/Al show usually a good correlation with the particle size data, and the alr(Si/Al) has been utilized as a high-resolution grain size proxy. Increasing Si/Al ratios are related to an increasing amount of coarse-grained material, whereas an decreasing trend points to a fining-upward interval. Note that the grain size proxies Zr/Rb and Si/Al largely co-vary throughout the studied section implying that the silica in the system is largely of detrital origin

and sandstones. Above the sandstone interval, upper Valanginian to lowermost upper Hauterivian sediments are similar to those of the composite section consisting of rather monotonous dark grey-coloured fine mudstones (Figure 5). However, the average proportion of sand (63–2,000 μm) and coarse silt (20–63 μm) is with nearly 8 wt% twice as high as in the coeval interval of the composite section.

The CaCO$_3$ content varies widely from less than 1 wt% to more than 50 wt%, with an average around 14 wt% (Figures 3 and 5). The average CaCO$_3$ content is thus slightly higher than in coeval sediments from the more distal basinal section (Ø: 10 wt%). Pale-dark bedding rhythms similar to those observed in the basin centre are quite common in the middle lower Hauterivian (Figure 5). The C$_{org}$ content of the fine mudstones varies between 0.3 and 1.8 wt%, whereby the highest values occur around the lower Hauterivian – upper Hauterivian boundary (Figure 5).

5.2 | Geochemical characteristics—XRF CS

In total more than 48,000 XRF-CS data points per element (Al, Si, S, Cl, K, Ca, Ti, Mn and Fe) were finally acquired for all four studied cores. This high-resolution geochemical data set provides an outstanding opportunity to capture the facies heterogeneity present within the mudstone-dominated Lower Cretaceous succession in the eastern part of the LSB.

5.2.1 | Silicon/Aluminum

A comparison of discrete grain size analyses with XRF scanning data suggests that the additive log ratio of Si/Al represents a suitable grain size proxy for the studied successions (Figures 4 and 5). Apart from certain intervals, alr(Si/Al) and grain size measurements show a very similar pattern.

In the central part of the LSB sediments of the uppermost Berriasian to lowermost Valanginian are generally characterized by comparably low Si/Al ratios, except for a small segment between 423 and 418 mcd which shows slightly higher values (Figure 4). A long-term increasing trend is observed in the lower Valanginian to lowermost upper Valanginian, reaching maximum values at about 355 mcd (Figure 4). High values of alr(Si/Al) prevail in the upper Valanginian up to a depth of around 315 mcd. An abrupt shift towards lower Si/Al ratios can be observed in the depth interval between 315 and 295 mcd, followed by an increasing trend towards the Valanginian–Hauterivian boundary. The lower Hauterivian section shows an overall decreasing trend, reaching particularly low Si/Al values close to the lower Hauterivian–upper Hauterivian boundary at around 145 mcd. The succeeding upper Hauterivian shows a return to higher Si/Al ratios, reflected by a gradually increasing trend up to around 90 mcd. For the remaining upper Hauterivian, the Si/Al curve shows again a decreasing trend. This decrease continues into the lower Barremian, followed by increasing values in the upper part of the Barremian to lowermost Aptian. A slightly
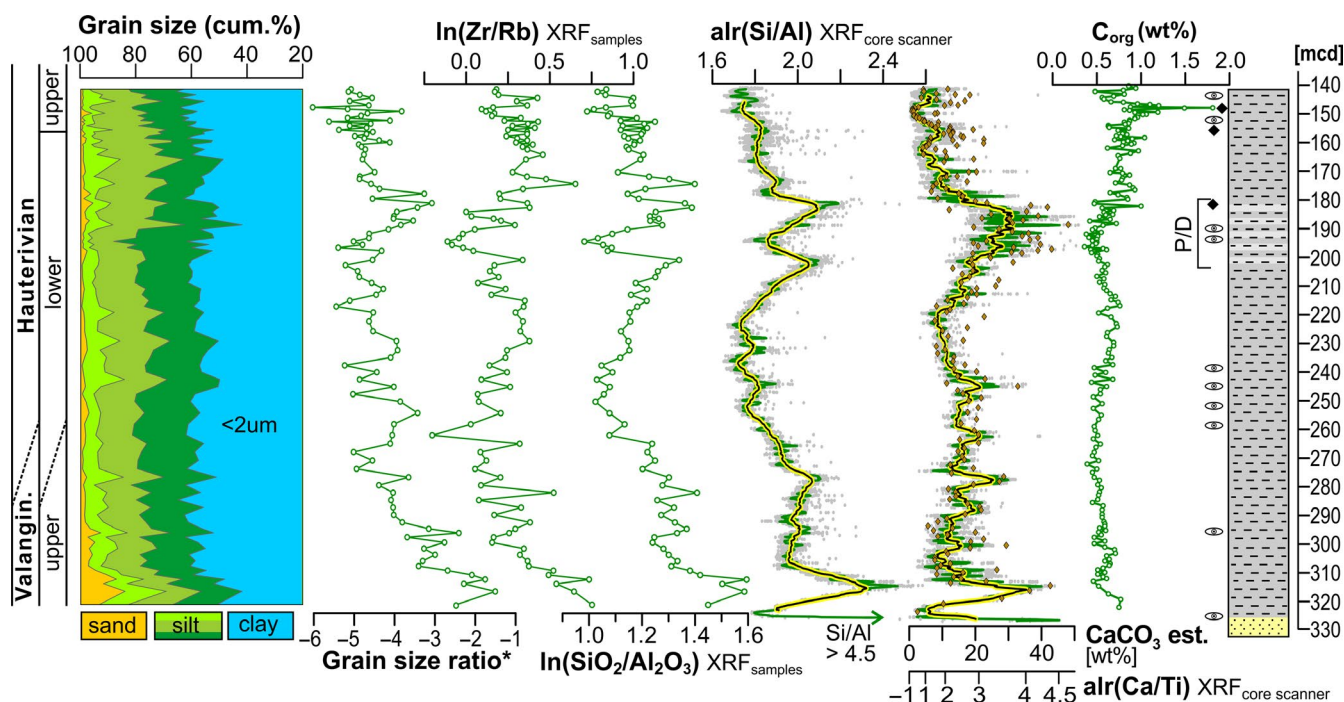

FIGURE 5 Grain size data, selected element ratios obtained by XRF core scanning (Si/Al and Ca/Ti) and conventional XRF measurements (Zr/Rb and Si0$_2$/Al$_2$O$_3$), C$_{org}$ content, as well as the lithology of the Zuckerfabrik 2 core

decreasing trend in alr(Si/Al) is observed in the lower Aptian above 38 mcd.

For the proximal Zuckerfabrik 2 core the Si/Al values are about 0.1 and 0.2 higher than for the composite record, but the trends are comparable between the two records (Figures 5 and 6). The sandy Valanginian sediments (109–113 m) are reflected by the highest Si/Al ratios recorded, followed by a sudden decline in Si/Al ratios at the contact between the

sandstones and overlying mudstones (Figure 5). A short excursion to higher ratios is observed in the succeeding interval between 109 and 107 m. The remaining upper Valanginian shows a decreasing trend between 107 and 102 m, followed by increasing values towards the Valanginian–Hauterivian boundary. An overall decrease in Si/Al ratios can be observed in the lowermost Hauterivian, reaching minimum values at around 75 m. The middle lower Hauterivian shows a return
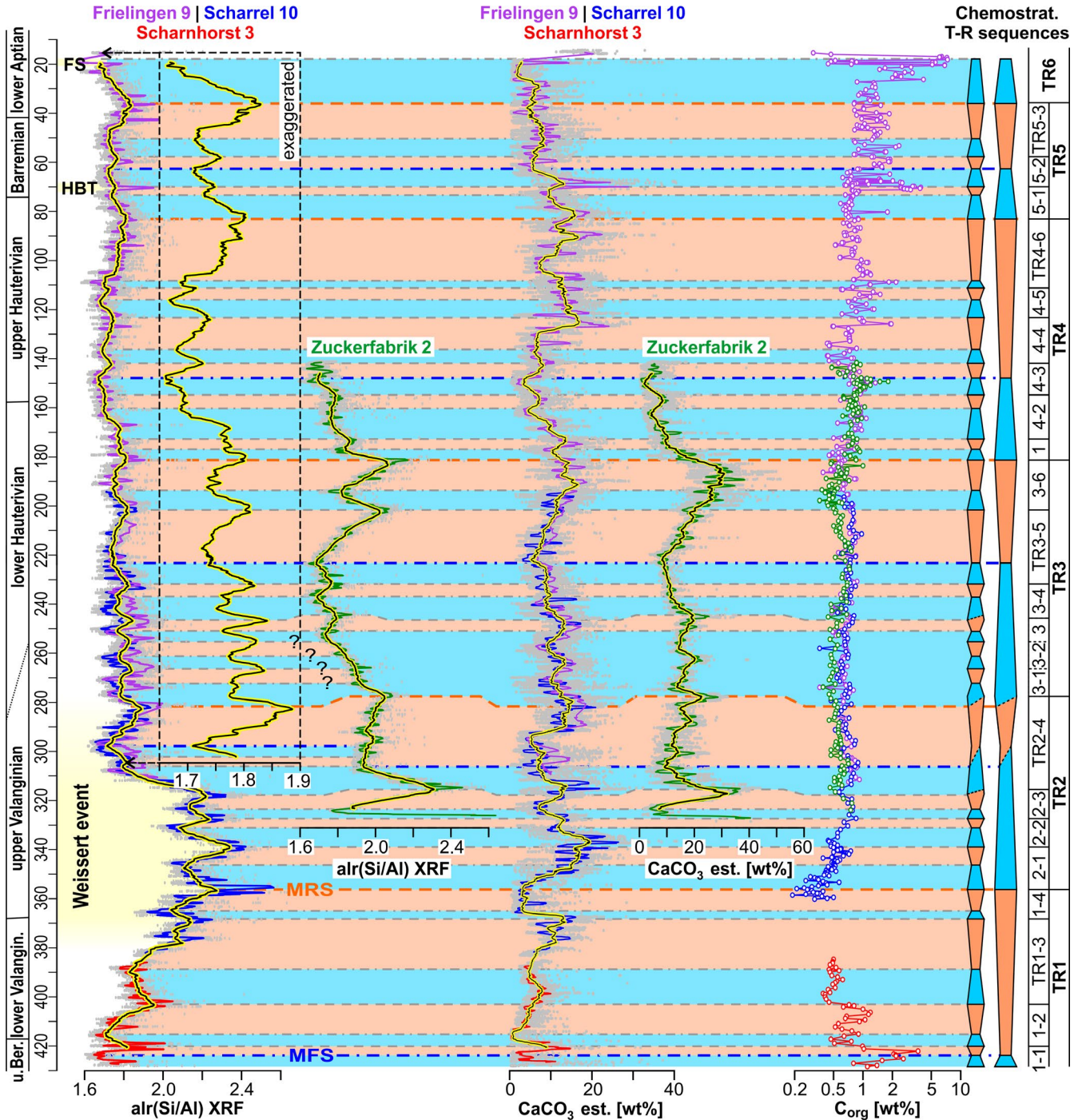

FIGURE 6 Geochemical (Si/Al, Ca/Ti and C$_{org}$) records of the studied drill cores with sequence stratigraphic interpretation. FS, Fischschiefer; HBT, Hauptblätterton; mcd, metres composite depth; MRS, maximum regressive surface; MFS, maximum flooding surface; RST, regressive systems tract; TR, T-R sequence; TST, transgressive systems tract sensu Embry (1993) and Embry and Johannessen (1993)

to higher Si/Al ratios, reflected by an increasing-decreasing-increasing trend. The highest Si/Al values are reached at around 45.5 m. The remaining lower to upper Hauterivian exhibits an overall decreasing trend punctuated by phases of slightly increasing Si/Al ratios. Particularly low Si/Al values have been reached around the lower Hauterivian–upper Hauterivian boundary.

5.2.2 | Calcium/Titanium

The additive log ratio Ca/Ti was used to estimate down-core variations in the $CaCO_3$ content. Carbonate-poor intervals are commonly related to low alr(Ca/Ti), whereas high ratios are interpreted to represent carbonate-rich sections. The Ca/Ti ratio shows a high variability over the studied Lower Cretaceous succession, with some long-term increasing and decreasing trends (Figure 3).

In the composite record from the central part of the LSB $CaCO_3$ est. contents fluctuate between 0 and 45 wt% with an average value of around 10 wt% (Figure 4). The Berriasian interval shows comparably low Ca/Ti ratios, with an average $CaCO_3$ est. content of 5 wt%. Furthermore, a gradual decrease in alr(Ca/Ti) is observed towards the Berriasian–Valanginian boundary, reaching minimum values in the lowermost Valanginian. After this interval with significantly low ratios, an increasing trend is observed for the remaining lower Valanginian, reaching $CaCO_3$ est. contents of over 15 wt%. This trend is interrupted around the lower–upper Valanginian boundary (Figure 4), and followed by an interval characterized by particularly low Ca/Ti ratios (352–367 mcd). The succeeding upper Hauterivian shows a return to higher Ca/Ti ratios, reaching maximum values at around 355 mcd. The $CaCO_3$ est. content rises partly to over 30 wt%. A stepwise decrease in the Ca/Ti ratio occurs in the depth interval between 336 and 293 mcd, followed by an increasing trend towards the Valanginian–Hauterivian boundary. An overall decrease in the Ca/Ti ratio can be observed again in the upper part of the lower Hauterivian, followed by increasing values in the interval between 221 and 194 mcd. The remaining lower Hauterivian exhibits a strong decrease in the Ca/Ti ratio. Particularly low Ca/Ti values have been reached around the lower Hauterivian–upper Hauterivian boundary (Figures 3 and 4). Mudstones are here largely carbonate-free. After this interval with particularly low ratios, an increasing trend is observed for the earliest upper Hauterivian, reaching $CaCO_3$ est. contents of over 15 wt%. For the remaining upper Hauterivian, the Ca/Ti curve shows no clear trend, whereby fluctuations in the ratio are of higher amplitude than in the underlying sediments. The lowermost Barremian is characterized by comparably high Ca/Ti values between 71 and 67 mcd. In this interval a distinct paper shale horizon occurs, the so-called Hauptblätterton. The $CaCO_3$ est. contents rise partly to over 45 wt%. The remaining Barremian to lower Aptian interval is generally characterized by lower and highly variable Ca/Ti ratios. Whereby, an abrupt increase in the Ca/Ti ratio occurs in the uppermost section of the Frielingen 9 core, showing particularly high Ca/Ti values. These high ratios are correlated to the strongly bioturbated marly sediments observed at the top of the Frielingen 9 core.

In the eastern part of the LSB, the Zuckerfabrik 2 core displays $CaCO_3$ est. between 0 and 50 wt%, with an average value of around 14 wt% (calcareous concretions excluded; Figures 3 and 5). The upper Valanginian mudstones directly overlying the sandy interval (109–113 m) are characterized by a highly variable $CaCO_3$ est. content, ranging from less than 5 to more than 40 wt%, thereby showing an overall decreasing trend (102.5–109.0 m). The remaining upper Valanginian to lowermost Hauterivian shows again an increase, followed by decreasing $CaCO_3$ est. contents in the interval between 78 and 69.5 m. The middle lower Hauterivian is characterized by a strong increase in the Ca/Ti ratio. Particularly high $CaCO_3$ est. contents are recorded in the interval between 60 and 45 m, with an average value of around 28 wt%. A stepwise decrease in the Ca/Ti ratio can be observed in the remaining lower Hauterivian. The lowest ratios are found around the lower Hauterivian–upper Hauterivian boundary. Above this interval with particularly low ratios, a slightly higher carbonate content is observed for the earliest upper Hauterivian.

6 | DISCUSSION

6.1 | Evaluation of Si/Al as a grain proxy

It is well known that the geochemical composition of siliciclastic sediments correlates strongly with grain size (Bloemsma *et al.*, 2012). This is because chemical alteration and mechanical breakdown of source rocks, followed by sorting of particles during transport and deposition, lead to preferential enrichment of specific mineral phases in certain grain size fractions (Weltje and von Eynatten, 2004). Given the strong influence of grain size on sediment inorganic geochemistry, single element variations measured by, for example, XRF CS are increasingly used to estimate grain-size variations at high resolution in sediment cores. For example, changes in the grain size have been previously inferred from a number of elemental ratios, including Si/Al (Calvert and Pedersen, 2007). The Si/Al ratio is generally assumed to represent the ratio of quartz (rich in Si) to clay (rich in Al) in most fine-grained siliciclastic sediments (Sano *et al.*, 2013; Clift *et al.*, 2014; Rowe *et al.*, 2017). As quartz is more abundant in the coarse fraction than in the fine fraction (Cuven *et al.*, 2010), the Si/Al ratio is typically considered to be a useful proxy for grain size. However, interpretation of XRF-CS data is not straightforward, and not every elemental proxy can be generalized and transferred to other study regions.

Si/Al ratios and grain size measurements were compared to test whether variations in Si/Al ratios mirror textural parameters in the studied succession. In Figures 4 and 5 grain size data are plotted as cumulative proportions of particle sizes as well as log ratios of a coarse fraction consisting of particles having a size between 63 and 630 μm (fine to medium sand) to a fine fraction consisting of clay to coarse silt (<63 μm). Apart from certain intervals, a good correlation between Si/Al and calculated grain size ratios can be observed. Increasing Si/Al ratios are commonly associated with an increase in the sand fraction, whereas decreasing Si/Al values coincide with decreasing contents of sand (Figures 4 and 5). Furthermore, sediments from the Zuckerfabrik 2 core show slightly higher Si/Al ratios as contemporaneous units from the distal basinal composite section. This most likely reflects the higher average proportions of sand (63–2,000 μm) and coarse silt (20–63 μm) which has been recognized in the more proximal Zuckerfabrik 2 core.

Marked divergences between Si/Al ratios and measured grain sizes occur in the uppermost Berriasian and the lower Aptian. Both intervals are characterized by coarser grain sizes (up to 57 wt% sand-size), however, Si/Al values are rather low indicating that these intervals are not particularly rich in quartz. This is supported by the lack of correlation with SiO_2 contents measured by conventional WD-XRF analyses. Compared to the remaining succession, C_{org} values as well as Fe_2O_3 and SO_3 contents are considerably elevated in these two intervals (see also Data S1). The high Fe_2O_3 and SO_3 values most likely correspond to increased pyrite contents, and indeed pyrite in the form of scattered crystals, small nodules and tiny lenses is quite common, especially in the lower Aptian. Numerous studies showed that early diagenesis, in particular the precipitations of cements such as pyrite, may lead to an apparent grain-size increase (Macquaker and Taylor, 1996; Schieber, 1996; Schieber et al., 2000; Schieber and Baird, 2001), and thus obscure the original grain size of the sediments.

Even though Si/Al ratios dominantly reflects grain size changes (Figures 4 and 5), the use of Si/Al ratios as a grain size proxy should be treated with caution, because it presupposes that all the quartz is mainly of detrital origin. However, larger SiO_2 components can also be contributed by biogenic silica, and Si/Al ratios have been therefore used in some studies as a measure for biogenic silica production (Dickson et al., 2010). For the studied succession, it is reasonable to relate increasing Si counts predominantly to higher abundances of detrital quartz due to the following factors: (a) Silica-producing organisms such as radiolarians are almost absent in the studied residuals used for micro-palaeontological dating and (b) Si/Al and Zr/Rb ratios covary throughout the studied sections (Figures 4 and 5). Like Si/Al, the Zr/Rb ratio has been used as a sediment grain-size proxy in numerous studies (Dypvik and Harris, 2001; Chen et al., 2006; Kylander et al., 2011; Wang et al., 2011).

Zirconium occurs in sediments almost exclusively as the mineral zircon ($ZrSiO_4$), a dense resistant mineral, which is commonly transported with silt and sand-sized quartz in the detrital fractions. In contrast, Rb is often enriched in clay minerals where it substitutes for K (Calvert and Pedersen, 2007). Given that Zr mainly occurs in sediments as detrital grains, a strong correlation between Si/Al and Zr/Rb ratios implies that the silica in the system is related to zircon in the system and thus is of detrital origin. Because biogenic silica content is negligible in the studied succession and Si/Al ratios generally show a good correlation with grain sizes, the XRF-CS derived Si/Al record represents a reliable grain size proxy for the studied mudstones.

6.2 | Establishing a sequence stratigraphic framework

Stratigraphic trends in grain size are an integral part of many sequence stratigraphic analyses and are commonly used to discern between progradational and retrogradational trends in marine successions (Catuneanu, 2006). As one of the first, Macquaker et al. (1998) have clearly demonstrated that this approach is also applicable in distal basinal settings, and not limited to marginal, coarser grained systems as they utilized large-scale fining-upward and coarsening-upward successions within the Kimmeridge Clay Formation to define transgressive and regressive systems tracts (RSTs). In recent years, geochemical proxies indicative of coarser clastic input (e.g., Si/Al, Zr/Al and Zr/Rb) have been increasingly used to delineate sequences and their component systems tract in fine-grained successions (Ver Straeten et al., 2011; Turner et al., 2015, 2016), and a similar approach has been applied in the current study to develop a sequence stratigraphic framework for the Lower Cretaceous mudstone-dominated succession in the eastern LSB. In this regard, an important first step was to evaluate whether geochemical variation determined by XRF-CS measurement can be used to characterize the studied cores in terms of variations in grain size.

The transgressive-regressive (T-R) Model of Embry (1993) and Embry and Johannessen (1993) has been applied to carry out the sequential subdivision of the mudstone-dominated Lower Cretaceous succession in the eastern LSB. Individual T-R sequences are bounded by maximum regressive surfaces (MRSs) in the marine realm, whereas maximum flooding surfaces (MFSs) are used to subdivide the T–R sequences into transgressive and RSTs. In the present study, vertical grading trends inferred from Si/Al changes were used to identify transgressive and regressive episodes within the mudstone-dominated succession. Large-scale upward-fining intervals (decreasing Si/Al ratios) were used to define transgressive systems tracts (TSTs) and the level at which the stacking patterns change from upward-fining to upward-coarsening as MFSs. Conversely, large-scale upward-coarsening packages

(increasing Si/Al ratio) are interpreted as RSTs and the tops of these coarsening-upward trends as MRSs. According to these criteria, six T-R sequences and 23 T-R subcycles have been recognized within the studied uppermost Berriasian to lower Aptian mudstone-dominated succession (Figure 6).

6.3 | Correlation of T-R sequences

Utilizing grain size variations and trends is generally a viable method to identify T-R sequences in individual outcrops or cores, but matching such sequences across a basin, solely based on the observed grading trends, is not necessarily a reliable correlation technique. Changes in sedimentation patterns across a basin make it difficult to know which stratigraphic sequences are age-equivalent when comparing vertical profiles from different sections. To constrain sequence stratigraphic correlations an independent time control is therefore vital, especially in the case of a sparse and discontinuous data base such as one built by isolated outcrops, core or well logs (Catuneanu, 2006). In the present study, an independent and detailed core-to-core correlation among sites was achieved by integrating XRF elemental data with isotope and biostratigraphy (Figure 3). The core-to-core correlation, which was mainly established based on distinct trends in the K/Ti records, enable a robust, largely objective correlation of T-R sequences and their component systems tract among the studied sections. Furthermore, the correlation shows that most MRSs and MFSs have good lateral continuity and can be correlated from the distal basinal composite section to the more proximal Zuckerfabrik 2 core (Figure 6).

6.4 | Transgressive-regressive cycles in the LSB and adjacent areas

The recognized T-R sequences (TR1-TR6) and their subcycles are briefly described and compared to previous studies in the LSB and adjacent areas in order to better assess the reliability of the established sequence stratigraphic framework. Figure 7A and B illustrates, among other things, the relationship between sequences defined by Hoedemaeker and Herngreen (2003) and the results presented here. Hoedemaeker and Herngreen (2003) presented a detailed correlation chart, comparing the Tethyan Berriasian to Barremian successions of Spain and France with the Boreal strata of England, Germany and the Netherlands, which is a well-funded basis and useful for an evaluation of the established sequence stratigraphic framework.

6.4.1 | TR1 sequence (upper Berriasian – Lowermost upper Valanginian)

The uppermost Berriasian to lowermost Valanginian is characterized by rather low Si/Al values, and two MFSs are recognized throughout this interval (Figure 6). The MFS of the basal T-R sequence (TR1 MFS) is particularly prominent and placed at a Si/Al minimum in the uppermost Berriasian at about 422 mcd. The second MFS is developed after a minor transgression (TR1-2 TST) in the lowermost Valanginian. Mudstones close to the distinct TR1 MFS are characterized by elevated C_{org} (up to 5.4 wt%).

The observed transgressive nature of the uppermost Berriasian to lowermost Valanginian is well known and has previously been described in a number of studies. The LSB was largely separated during the Berriasian from marine influence, and non-marine deposits up to 700 m thick were accumulated under a brackish-lacustrine regime (Mutterlose et al., 1997; Mutterlose and Bornemann, 2000; Schneider et al., 2018). However, a gradual shift towards a more marine influenced setting occurred in the upper part of the Berriasian (Martin, 1961; Kemper, 1973), and in the earliest Valanginian the LSB became fully marine, documented by ammonite-bearing strata (Mutterlose, 1992; Mutterlose and Bornemann, 2000). This prominent transgression is also evident in the southern North Sea Basins by an overall retrogradational facies pattern, and two fairly prominent flooding surfaces (FS; Jeremiah et al., 2010). The lower one (FS1) is dated with macrofossils as lying within the uppermost Berriasian albidum Zone whilst palynological data confirm an earliest Valanginian age (lower Paratollia Zone) for FS2 (Jeremiah et al., 2010). The upper part of the albidum Zone is equivalent to the German Wealden 6 ostracod Biozone used in this paper (Schneider et al., 2018), and thus FS1 of Jeremiah et al. (2010) probably correlates to the distinct MFS of sequence TR1. Furthermore, the earliest Valanginian FS2 (named Lower Paratollia MFS; Jeremiah et al., 2010) may correspond to the MFS recognized at the base of the Valanginian (TR1-2 MFS; Figure 6).

The transgression observed around the Berriasian–Valanginian boundary is followed by a distinct regressive phase throughout the remaining lower Valanginian to lowermost upper Valanginian (TR1 RST) evident by a distinct increase in Si/Al ratios and diminished C_{org} (Figure 6). The MRS bounding the top of sequence TR1 is placed at the Si/Al peak corresponding with the highest measured Si/Al values of the composite section. Four T-R subcycles are distinguishable in the lower Valanginian TR1 sequence based on variations in the Si/Al record. These subcycles can be correlated to some extent with distinctive marine sandstone horizons that have been deposited along the margin of the LSB. In the eastern part of the basin, adjacent to the study area, Bartenstein and Brand (1951) recognized four sandstone horizons in the Valanginian whose occurrence tightly correlates with the timing of high Si/Al ratios in the studied cores. The earliest sandstone horizon was stratigraphically assigned to the middle lower Valanginian and, thus,
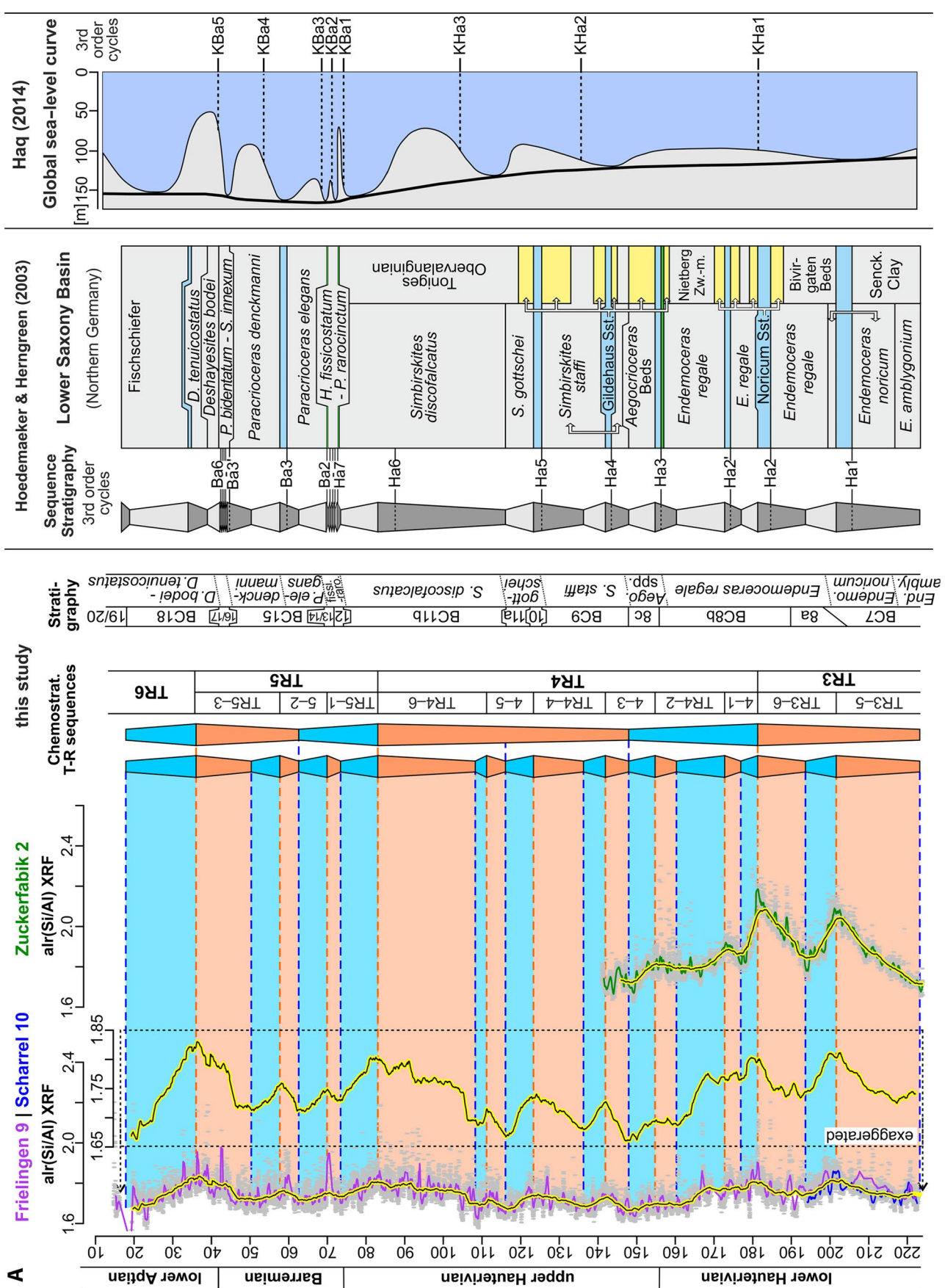
FIGURE 7 (A and B) Comparison of T-R sequences identified based on variations in alr(Si/Al) (this study) with depositional sequences defined by Hoedemaeker and Herngreen (2003) for the LSB, as well as with the global sea-level curve of Haq (2014)
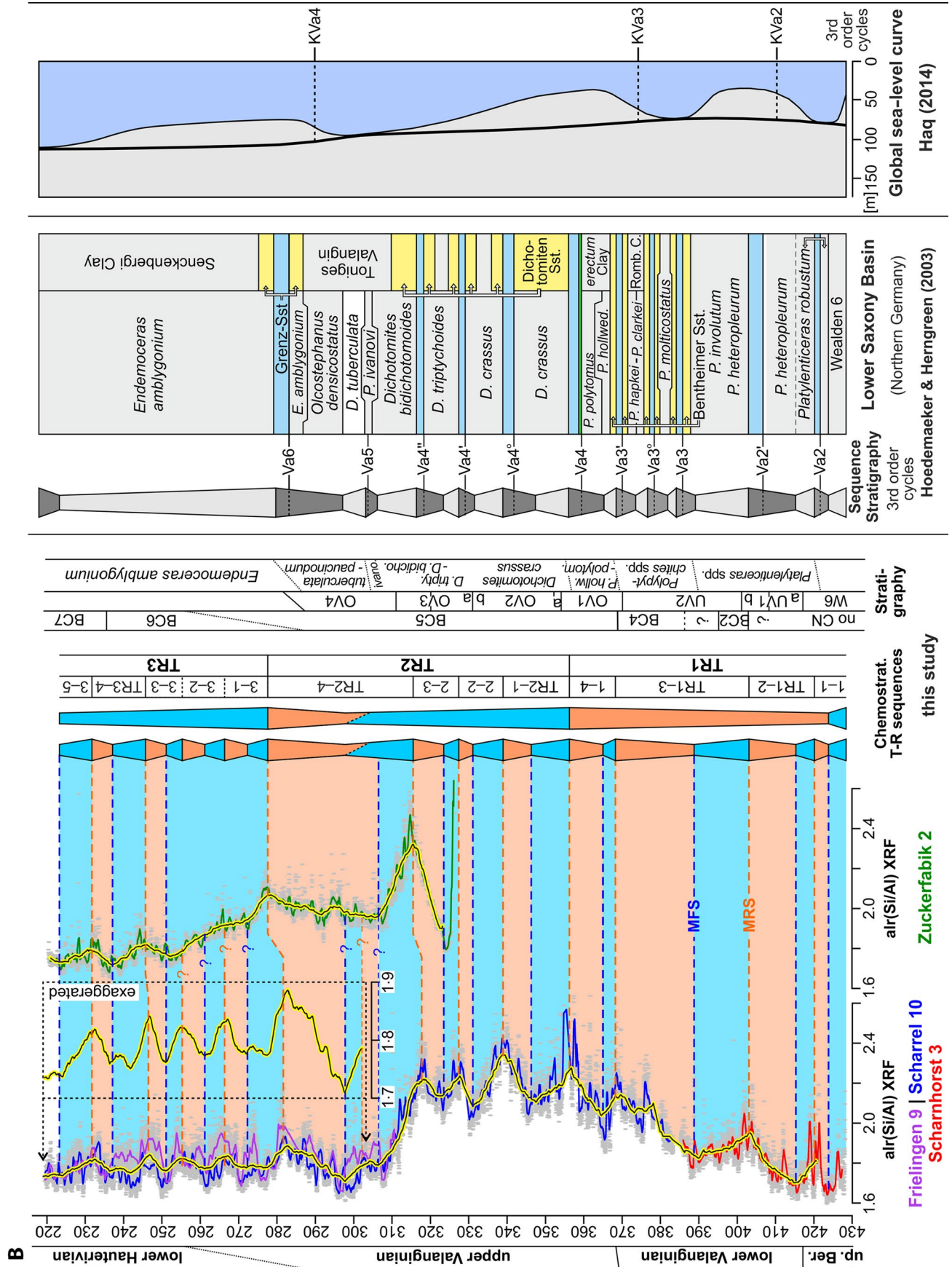
FIGURE 7 (Continued)

correlates closely with the comparably high Si/Al ratios observed in the depth interval around 402 mcd. Progradation of this early Valanginian sandstone is most likely related to the TR1-2 RST (Figure 7B). Another prominent sandstone horizon representing the Bentheim Formation was deposited during the upper lower Valanginian in the western part of the LSB (Mutterlose, 1992; Mutterlose and Bornemann, 2000; Hoedemaeker and Herngreen, 2003)(Figure 7B). The Bentheim Formation is composed of several sheet-like sand bodies up to 80 m thick and has been described in detail by various authors (Kemper, 1976; Wonham *et al.*, 1997; Stadtler, 1998; Peksa *et al.*, 2015). According to Wonham *et al.* (1997) and Stadtler (1998) these sandstones can be differentiated into three genetic sequences, bounded by biostratigraphically defined MFSs. One of these MFSs is located at the base of the Bentheim Formation and represents a regional flooding surface (Upper Paratollia MFS; Jeremiah *et al.*, 2010). A correlation between this surface which has been identified in the western LSB and the MFSs defined in this study is very tentative but may corresponds to the MFS of sequence TR1-3 in the middle lower Valanginian.

It is generally assumed that a widespread transgression in the uppermost lower Valanginian abruptly terminated the deposition of the Bentheim Formation in the LSB (Ruffell, 1991; Jeremiah *et al.*, 2010), and that this transgression represents an important flooding event throughout the southern North Sea Basin (Jeremiah *et al.*, 2010) and in large parts of Europe (Rawson and Riley, 1982; Mutterlose and Bornemann, 2000; Copestake *et al.*, 2003). However, this transgressional event is not clearly traceable in the data reported here, which shows only a minor transgressional event (TR1-4 MFS) in the uppermost lower Valanginian marked by a moderate decline in the Si/Al ratio (Figure 6). Instead, a prominent regression is recognized around the lower Valanginian–upper Valanginian boundary (TR1-4 RST) evident by a sharp increase in Si/Al ratios and the deposition of sandy mudstones to muddy sandstones (Figure 4). This is in accordance with Bartenstein and Brand (1951) who describe a particularly prominent and laterally extensive sandstone horizon in the uppermost lower Valanginian. According to Hoedemaeker and Herngreen (2003), a major sea-level fall occurred during this time and generated the type 1 sequence boundary Va4. The regression associated with this prominent sea-level fall most likely corresponds to the RST of sequence TR1-4 (Figure 7B). Furthermore, this distinct regressive phase coincides roughly with the onset of the Valanginian Weissert event (positive shift in δ^{13}C; Figure 3), and thus support the conclusions of Kuhn *et al.* (2005), Duchamp-Alphonse *et al.* (2007) and Westermann *et al.* (2010) that the initial interval of the Weissert event coincided with a significant increase in terrigenous influx. Further evidence of sudden influx of siliciclastic material has been reported in the North Atlantic and the Tethyan domains. According to Weissert (1990), the increase in siliciclastics can be linked to intensified weathering processes in the source areas due to acceleration in the hydrological cycle under greenhouse conditions.

6.4.2 | TR2 sequence (upper Valanginian–lowermost Hauterivian)

The overlying TST of sequence TR2 displays an overall decreasing Si/Al signature coincident with decreasing C_{org} contents (Figure 6). Based on variations in the Si/Al record, three T-R subcycles are distinguishable in the Upper Valanginian TR2 sequence between 356 and 315 mcd. These regressive-transgressive episodes (TR2-1 to TR2-3) most likely mirror the distal influence of the Upper Valanginian Nienhagen Formation (formerly known as Dichotomiten-Sandstein or Valendis-Sandstein). This sandstone is associated with a short regressive trend (Ruffell, 1991; Mutterlose, 1992; Mutterlose *et al.*, 1997). According to Hoedemaeker and Herngreen (2003), the Nienhagen Formation can be differentiated into three main prograding sandstone tongues separated by transgressive intervals (Figure 7B), and the RSTs of sequences TR2-1 to TR2-3 (this paper) most likely correspond to the progradational phases of the different sandstone horizons. It appears that the deposition of the Nienhagen Formation has been abruptly terminated by a marked transgression in the uppermost Valanginian, as documented by the sudden decline in Si/Al ratios above 315 mcd (TR2-4 TST; Figure 7B). Furthermore, the sharp contact between the sandstones and the overlying mudstones in the Zuckerfabrik 2 core can be interpreted as indicative of an abrupt deepening (Figure 5). An uppermost Valanginian transgressive phase has been previously described in Ruffell (1991) and Mutterlose *et al.* (1997), among others, for the LSB. This transgression has been deduced by these authors from an influx of both Tethyan nannofloras and faunas into the LSB.

The abrupt transgression is followed by a regressive phase throughout the remaining upper Valanginian to lowermost Hauterivian (TR2 RST), whereby the onset of the regression seems to be diachronous, becoming younger towards the basin centre (Figure 6). A minor regression close to the Valanginian–Hauterivian boundary has been previously described for the western part of the LSB (~80 km distance) and is evident by the deposition of the Grenz-Sandstone (Ruffell, 1991; Mutterlose, 1992; Mutterlose *et al.*, 1997). According to Hoedemaeker and Herngreen (2003) the Grenz-Sandstone can be interpreted as a sandstone tongue consisting of a prograding base and a retrograding top part. Progradation of the Grenz-Sandstone is most likely related to the RST of sequence TR2 (Figure 7B).

6.4.3 | TR3 sequence (lower Hauterivian)

The lowermost Hauterivian interval between 280 and 220 mcd shows an overall transgressive development (TR3 TST) superimposed by a series of minor regressions and transgressions. This transgression is clearly apparent within the Zuckerfabrik 2 core by a sharp decrease in Si/Al ratios coincident with increasing C_{org}. Within the more distal basinal composite section the transgression is less distinct and five T-R subcycles are differentiated in this interval (Figure 6). The MRSs of these subcycles show similar Si/Al values and no clear transgressive or regressive trend can be deduced. However, the decreasing Si/Al values of the MFSs indicate that this interval shows overall transgressive tendencies. A lowermost Hauterivian transgression that reached its maximum in the basal Hauterivian *Endemoceras amblygonium* ammonite Zone similar to those observed in this study has been previously described for the LSB (Mutterlose, 1992; Mutterlose *et al.*, 1997; Mutterlose and Bornemann, 2000). A coeval flooding event is also evident in the southern North Sea basins by an overall retrogradational facies pattern, and a fairly prominent MFS has been calibrated to the *E. amblygonium* ammonite Zone (Amblygonium MFS; Jeremiah *et al.*, 2010). The distinctive MFS of sequence TR3 most likely coincides with the Amblygonium MFS of Jeremiah *et al.* (2010), or rather with the MFS of sequence Va6 of Hoedemaeker and Herngreen (2003)(Figure 7B).

Regressive tendencies evident by a renewed progradation of coarser clastics into the southern North Sea basins have been observed above the lowermost Hauterivian Amblygonium MFS, and in the middle Upper Hauterivian the first siliciclastics, known in Germany as the Noricum Sandstone (Georgsdorf Formation), were deposited locally in the LSB (Jeremiah *et al.*, 2010). The Georgsdorf Formation can be divided into two tongues (Kemper, 1976), each consisting of a prograding lower and a retrograding upper part. The stratigraphic position of this sandstone is, however, not well constrained in the literature. In several publications, these sandstones have been stratigraphically assigned to the *Endemoceras noricum* ammonite Zone (Kemper, 1976; Mutterlose, 1992; Möller and Mutterlose, 2014). According to Kemper (1992) and Hoedemaeker and Herngreen (2003), the Georgsdorf Formation does not belong to the *E. noricum* Zone but is restricted to the overlying *Endemoceras regale* Zone (Figure 7A). Lithologically, the Georgsdorf Formation is generally characterized by marly, fine-grained sandstones to very fine-sandy marlstones (Kemper, 1976, 1992). A distinctly more calcareous interval is recognized in the middle lower Hauterivian, as depicted by the $CaCO_3$ est. record (Figure 6). Two T-R subcycles are distinguishable in this interval spanning the *noricum* to *regale* ammonite Zones. These regressive-transgressive episodes are most

likely time-equivalent to the deposition of the Georgsdorf Formation in the study area and the RSTs of sequences TR3-5 to TR3-6 correspond to the progradational phases of the different sandstone horizons (Figure 7A).

6.4.4 | TR4 sequence (middle lower Hauterivian to upper Hauterivian)

The observed regressive tendencies in the middle lower Hauterivian are terminated by a prominent mid-Hauterivian transgression (TR4 TST). This transgressive phase, which culminated around the lower Hauterivian–upper Hauterivian boundary, is evident by a clear decline in Si/Al ratios accompanied by a gradual decrease in the $CaCO_3$ est. content and an increase of C_{org} (Figure 6). The highest concentrations of C_{org} are recorded at the MFS at the top of the TR4 TST (up to 1.8 wt%), which is placed at a distinct Si/Al minimum at around 149 mcd. The transgressive trend observed in the upper lower Hauterivian agrees with previous studies from the LSB, which found clear evidence for a widespread transgression during this time (Mutterlose, 1992; Mutterlose and Ruffell, 1999; Mutterlose and Bornemann, 2000). This transgressive phase which has been recognized over much of northwest Europe (Kemper *et al.*, 1981; Rawson and Riley, 1982; Ruffell, 1991; Herngreen and Wong, 2007) is distinguished, among other observations, by an extensive influx of both Tethyan nannofloras and faunas into the LSB (Mutterlose, 1992; Mutterlose *et al.*, 1997).

The mid-Hauterivian transgression, which may correspond to the transgressive interval of sequence KHa1 of Haq (2014), is followed by an overall regressive trend in the upper Hauterivian (RSTs of TR4; Figure 7A). These regressive tendencies in the Upper Hauterivian have been previously recognized by various authors and are evident in the LSB by a predominance of boreal and endemic taxa in this interval (Mutterlose, 1992; Mutterlose *et al.*, 1997; Mutterlose and Wiedenroth, 2009). Furthermore, the onset of this regressive phase is documented by a renewed progradation of coarser clastics into the LSB. These sandstone units, known in Germany as the Gildehaus Formation, can be differentiated into three main prograding sandstone tongues, separated by transgressive intervals (Hoedemaeker and Herngreen, 2003). Their basal part has recently been assigned to the uppermost lower Hauterivian (upper BC8b Biozone; Möller and Mutterlose, 2014), and thus the TR4-2 RST probably documents the earliest progradational phase of the Mid-Hauterivian Gildehaus Formation (Figure 7A).

The overall regressive trend observed throughout the upper Hauterivian is punctuated by minor transgressive phases, including a distinct transgression in the middle upper Hauterivian (TR4-5 TST; Figure 7A). This transgressional phase probably correlates with the *gottschei-marginatus* ammonite Zone transgression, which terminated the deposition of

the Gildehaus Formation (Mutterlose, 1992). A largely coeval flooding event is also evident in the southern North Sea basins, and a prominent MFS has been calibrated to the *Simbirskites gottschei* ammonite Zone (Gottschei MFS; Jeremiah *et al.*, 2010). Based on biostratigraphic observation it is assumed that the TR4-5 MFS likely coincides with the *Gottschei* MFS of Jeremiah *et al.* (2010). After the middle upper Hauterivian transgression, the bulk of the remaining upper Hauterivian interval shows again an overall regressive nature evidenced by increasing Si/Al ratios (TR4-6 RST; Figure 6).

6.4.5 | TR5 and TR6 sequences (uppermost Hauterivian to lower Aptian)

The uppermost Hauterivian to lower Barremian is marked by another transgression which is documented by a gradual decrease in the Si/Al ratio (TR5 TST; Figure 6). A coeval transgressional phase has been reported by Mutterlose (1992) and Mutterlose and Bornemann (2000), among others, for the LSB. This transgression has been inferred by these authors from an extensive influx of both Tethyan nannofloras and faunas into the LSB. The transgressive nature of the uppermost Hauterivian to lower Barremian is also characterized by an overall retrogradational facies pattern in the southern North Sea basins, and two regional prominent MFSs have been calibrated to the Hauptblätterton facies in the eastern Netherlands and LSB (Fissicostatum and Elegans MFSs; Jeremiah *et al.*, 2010).

This interpretation, however, is in opposition to the findings reported here, based on the herein documented increase in grain size and the occurrence of a sandy horizon that interrupts the proximal paper shale facies in the Salzgitter area (eastern part of the LSB; Gerardi, 1986) it is tentatively suggested that the Hauptblätterton facies is related to a short-term regressive phase (TR5-1 RST, Figure 6). This is well in line with the idea that the Hauptblätterton was deposited in an oxygen-poor, restricted basin with sluggish circulation (Mutterlose and Böckel, 1998).

The observed transgressional phase in the uppermost Hauterivian to lowermost Barremian is followed by an overall regressive trend in the overlying Barremian to lowermost Aptian interval (TR5 RST; Figure 6). The overall regressive character of the Barremian in northwest Europe has often been quoted (Rawson and Riley, 1982; Ruffell, 1991; Mutterlose *et al.*, 1997; Mutterlose and Bornemann, 2000). In marginal areas of the LSB, the Barremian regression resulted in both erosion and non-deposition as well as the massive progradation of marine sandstones into the basin (Gravenhorst Member; Mutterlose and Bornemann, 2000). Further, westwards in the Netherlands, the regression is evident by the progradational De Lier Member that was laid down along the southern margin of the West Netherlands Basin (Herngreen and Wong, 2007).

The regression observed around the Barremian–Aptian boundary is followed by a distinct transgressive phase throughout the lower Aptian (TR6 TST) evident by a distinct decrease in Si/Al ratios. The MFS of sequence TR6 is placed at a Si/Al minimum corresponding with the highest measured C_{org} values of the studied succession (Figure 6). The high C_{org} contents are associated with the lower Aptian Fischschiefer; a paper shale horizon that is often interpreted as local expression of the global OAE 1a (Bottini and Mutterlose, 2012; Heldt *et al.*, 2012). The overall transgressive nature of the lower Aptian has been previously described and is mirrored in the LSB, among other things, by sandy–silty sediments in the north-western Teutoburger Wald (Mutterlose and Bornemann, 2000).

6.5 | Reliability of the sequence stratigraphic interpretation

The observed T-R sequences largely confirm previously recognized transgressive-regressive trends in the LSB and adjacent areas, and thus indicate the potential use of high-resolution elemental intensity data from XRF CS for developing sequence stratigraphic frameworks in mudstone-dominated successions. However, one of the concerns with building sequence stratigraphic frameworks based upon cyclicity is ensuring that the geochemical signal recorded is not a result of measurement errors or random 'noise' inherent in the system. For a reliable sequence stratigraphic interpretation, it is therefore important to determine whether the geochemical signals being measured represent a viable signal that is laterally persistent. Bearing this in mind, the most critical point of the sequence stratigraphic interpretation conducted during this study is that the results are partly based on a single composite section (Figure 6) which represents only a narrowly defined region in the distal part of the eastern LSB (Figure 1). In a single section it remains unclear whether the geochemical signal measured is laterally persistent, and therefore the identification of system tracts is more speculative and less reliable than using two or more sections along a proximal to distal transect. The detailed chemostratigraphic correlation of the studied cores, however, indicates that the geochemical variability present in the studied succession is for the overlapping core intervals laterally reproducible and correlatable across the eastern LSB (Figure 3). Furthermore, the correlation shows that most MRSs and MFSs have good lateral continuity and can be correlated from the distal basinal composite section to the more proximal Zuckerfabrik 2 core (Figure 6). This accordance in the overlapping intervals supports the assumption that the remaining parts of the composite section also preserve laterally persistent signals that can be used to generate a reliable sequence stratigraphic framework.

7 | CONCLUSIONS

The present study demonstrates the potential use of high-resolution elemental intensity data from XRF CS for generating and refining sequence stratigraphic frameworks in mudstone-dominated successions, using Lower Cretaceous seemingly monotonous mudstones from the depocentre of the LSB as an example.

1. An independent, detailed core-to-core correlation and the recognition of grain size variations and trends was the key to delineate sequences and their component systems tracts within these fine-grained rocks. A precise correlation among sites was achieved by integrating XRF elemental data with isotope and biostratigraphy. The elemental ratios of K/Ti in conjunction with Ca/Ti have proven to be particularly suitable in this regard, whereas variations and trends in the grain size were highlighted using Si/Al ratios. This ratio can be utilized in the present study as a high-resolution record of grain size variability because biogenic quartz is negligible in the studied succession.

2. Vertical grading trends inferred from Si/Al changes were used to identify transgressive and regressive episodes within the mudstone-dominated succession. Large-scale upward-fining intervals (decreasing Si/Al ratios) were used to define TSTs, and large-scale upward-coarsening packages (increasing Si/Al ratios) were interpreted as RSTs. Six transgressive–regressive (T-R) sequences were recognized based on variations in the Si/Al record. The observed T-R sequences largely confirm previously recognized transgressive-regressive trends in the LSB and adjacent areas.

3. The composite $\delta^{13}C_{org}$ record for the studied succession is in good accordance with existing Lower Cretaceous $\delta^{13}C$ curves and enables the identification of characteristic chemostratigraphic events. These include, among others, the Valanginian Weissert event that is characterized by a positive CIE. This event clearly corresponds to major changes in the grain size data, and its onset roughly agrees (~360 mcd) with a prominent regression in the uppermost lower Valanginian, and thus support the conclusions of earlier studies that the initial interval of this event coincided with a significant increase in terrigenous input.

CONFLICT OF INTEREST

We (the authors) have no conflict of interest to declare.

DATA AVAILABILITY STATEMENT

Data are available from PANGAEA (https://doi.org/10.1594/PANGAEA.898094).

ORCID

André Bornemann https://orcid.org/0000-0003-4341-2366

REFERENCES

Abouelresh, M. and Slatt, R. (2011) Shale depositional processes: example from the Paleozoic Barnett Shale, Fort Worth Basin, Texas, USA. *Central European Journal of Geosciences*, 3, 398–409.

Abouelresh, M.O. and Slatt, R.M. (2012) Lithofacies and sequence stratigraphy of the Barnett Shale in east-central Fort Worth Basin, Texas. *AAPG Bulletin*, 96, 1–22.

Aitchison, J. (1986) *The Statistical Analysis of Compositional Data*. London: Chapman & Hall Ltd, 416 pp.

Aplin, A.C. and Macquaker, J.H.S. (2011) Mudstone diversity: origin and implications for source, seal, and reservoir properties in petroleum systems. *AAPG Bulletin*, 95, 2031–2059.

Arnaud, F., Révillon, S., Debret, M., Revel, M., Chapron, E., Jacob, J. et al. (2012) Lake Bourget regional erosion patterns reconstruction reveals Holocene NW European Alps soil evolution and paleohydrology. *Quaternary Science Reviews*, 51, 81–92.

Bartenstein, H. and Bettenstaedt, F. (1962) Marine Unterkreide (Boreal und Tethys). In: Arbeitskreis der Mikropaläontologen (Ed.) *Leitfossilien der Mikropaläontologie*. Berlin: Gebr. Bornträger. pp. 225–297.

Bartenstein, H. and Brand, E. (1951) Mikropaläontologische Untersuchungen zur Stratigraphie des nordwestdeutschen Valendis. *Abhandlungen der Senckenbergischen Naturforschenden Gesellschaft*, 485, 239–336.

Betz, D., Führer, F., Greiner, G. and Plein, E. (1987) Evolution of the Lower saxony basin. *Tectonophys.*, 137, 127–170.

Bloemsma, M.R., Zabel, M., Stuut, J.B.W., Tjallingii, R., Collins, J.A. and Weltje, G.J. (2012) Modelling the joint variability of grain size and chemical composition in sediments. *Sedimentary Geology*, 280, 135–148.

Bohacs, K.M. and Schwalbach, J.R. (1992) Chapter II – sequence stratigraphy of fine-grained rocks with special reference to the Monterey Formation. In: Schwalbach, J.R., Bohacs, K.M. and White, L.D. (Eds.) *Sequence Stratigraphy in Fine-Grained Rocks: Examples from the Monterey Formation*. Bakersfield, CA: Society for Sedimentary Geology, Pacific Section, Bakersfield.

van den Boogaart, K.G. and Tolosana-Delgado, R. (2008) "compositions": a unified R package to analyze compositional data. *Computers and Geosciences*, 34, 320–338.

Bornemann, A. and Mutterlose, J. (2008) Calcareous nannofossil and δ¹³C records from the Early Cretaceous of the Western Atlantic Ocean: evidence for enhanced fertilization across the Berriasian-Valanginian transition. *Palaios*, 23, 821–832.

Bornemann, A., Erbacher, J., Heldt, M., Kollaske, T., Wilmsen, M., Lübke, N. *et al.* (2017) The Albian-Cenomanian transition and Oceanic Anoxic Event 1d – an example from the Boreal Realm. *Sedimentology*, 64, 44–65.

Bottini, C. and Mutterlose, J. (2012) Integrated stratigraphy of Early Aptian black shales in the Boreal Realm: calcareous nannofossil and stable isotope evidence for global and regional processes. *Newsletters on Stratigraphy*, 45, 115–137.

Bown, P.R., Rutledge, D.C., Crux, J.A. and Gallagher, L.T. (1998) Lower Cretaceous. In: Bown, P.R. (Ed.) *Calcareous Nannofossil Biostratigraphy*. London: Kluver Academic Publishers, pp. 86–131.

Calvert, S.E. and Pedersen, T.F. (2007) Elemental proxies for Palaeoclimatic and Palaeoceanographic variability in marine sediments: interpretation and application. *Development of Marine Geology*, 1, 567–644.

Catuneanu, O. (2006) *Principles of sequence stratigraphy*. Amsterdam: Elsevier Sciences, 386 pp.

Chen, J., Chen, Y., Liu, L., Ji, J., Balsam, W., Sun, Y. *et al*. (2006) Zr/Rb ratio in the Chinese loess sequences and its implication for changes in the East Asian winter monsoon strength. *Geochimica et Cosmochimica Acta*, 70, 1471–1482.

Clift, P.D., Wan, S. and Blusztajn, J. (2014) Reconstructing chemical weathering, physical erosion and monsoon intensity since 25Ma in the northern South China Sea: a review of competing proxies. *Earth Science Reviews*, 130, 86–102.

Copestake, P., Sims, A.P., Crittenden, S., Hamar, G.P., Ineson, J.R., Rose, P.T.*et al.* (2003) Lower Cretaceous. In: Evans, D., Graham, C., Armour, A. and Bathurst, P. (Eds.) *The Millenium Atlas: Petroleum Geology of the Central and Northern North Sea. Geological Society of London*, pp. 191–211.

Cuven, S., Francus, P. and Lamoureux, S.F. (2010) Estimation of grain size variability with micro X-ray fluorescence in laminated lacustrine sediments, Cape Bounty, Canadian High Arctic. *Journal of Paleolimnology*, 44, 803–817.

Dickson, A.J., Leng, M.J., Maslin, M.A. and Röhl, U. (2010) Oceanic, atmospheric and ice-sheet forcing of South East Atlantic Ocean productivity and South African monsoon intensity during MIS-12 to 10. *Quaternary Science Reviews*, 29, 3936–3947.

Diekmann, B., Hofmann, J., Henrich, R., Fütterer, D.K., Röhl, U. and Wei, K.-Y. (2008) Detrital sediment supply in the southern Okinawa Trough and its relation to sea-level and Kuroshio dynamics during the late Quaternary. *Marine Geology*, 255, 83–95.

Duchamp-Alphonse, S., Gardin, S., Fiet, N., Bartolini, A., Blamart, D. and Pagel, M. (2007) Fertilization of the northwestern Tethys (Vocontian basin, SE France) during the Valanginian carbon isotope perturbation: evidence from calcareous nannofossils and trace element data. *Palaeogeography, Palaeoclimatology, Palaeoecology*, 243, 132–151.

Dypvik, H. and Harris, N.B. (2001) Geochemical facies analysis of fine-grained siliciclastics using Th/U, Zr/Rb and (Zr+Rb)/Sr ratios. *Chemical Geology*, 181, 131–146.

Embry, A.F. (1993) Transgressive–regressive (T–R) sequence analysis of the Jurassic succession of the Sverdrup Basin, Canadian Arctic Archipelago. *Canadian Journal of Earth Sciences*, 30, 301–320.

Embry, A.F. and Johannessen, E.P. (1993) T–R sequence stratigraphy, facies analysis and reservoir distribution in the uppermost Triassic–Lower Jurassic succession, western Sverdrup Basin, Arctic Canada. In: Vorren, T.O., Bergsager, E., Dahl-Stamnes, Ø.A., Holter, E., Johansen, B., Lie, E. and Lund T.B. (Eds.) *Norwegian Petroleum Society Special Publications*, vol. 2. Amsterdam: Elsevier, pp. 121–146.

Erba, E., Bartolini, A. and Larson, R.L. (2004) Valanginian Weissert oceanic anoxic event. *Geology*, 32, 149–152.

Föllmi, K.B., Weissert, H., Bisping, M. and Funk, H. (1994) Phosphogenesis, carbon-isotope stratigraphy, and carbonate-platform evolution along the Lower Cretaceous northern Tethyan margin. *GSA Bulletin*, 106, 729–746.

Gerardi, J. (1986) *Bohrung Konrad 101 – Teil I geologischer Bericht*. Hannover: Bundesanstalt für Geowissenschaften und Rohstoffe.

Gröcke, D.R., Price, G.D., Robinson, S.A., Baraboshkin, E.Y., Mutterlose, J. and Ruffell, A.H. (2005) The Upper Valanginian (Early Cretaceous) positive carbon–isotope event recorded in terrestrial plants. *Earth and Planetary Science Letters*, 240, 495–509.

Hammes, U. and Frébourg, G. (2012) Haynesville and Bossier mudrocks: a facies and sequence stratigraphic investigation, East Texas and Louisiana, USA. *Marine and Petroleum Geology*, 31, 8–26.

Hammes, U., Hamlin, H.S. and Ewing, T.E. (2011) Geologic analysis of the Upper Jurassic Haynesville Shale in east Texas and west Louisiana. *AAPG Bulletin*, 95, 1643–1666.

Haq, B.U. (2014) Cretaceous eustasy revisited. *Global and Planetary Change*, 113, 44–58.

Heldt, M., Mutterlose, J., Berner, U. and Erbacher, J. (2012) First high-resolution δ13C-records across black shales of the Early Aptian Oceanic Anoxic Event 1a within the mid-latitudes of northwest Europe (Germany, Lower Saxony Basin). *Newsletters on Stratigraphy*, 45, 151–169.

Herngreen, G.F.W. and Wong, T.E.. (2007) Cretaceous. In: Wong, T.E., Batjes, D.A.J. and de Jager, J. (Eds.) *Geology of the Netherlands*. Amsterdam: Royal Netherlands Academy Arts and Sciences, pp. 127–150.

Hoedemaeker, P.J. and Herngreen, G.F. (2003) Correlation of Tethyan and Boreal Berriasian – Barremian strata with emphasis on strata in the subsurface of the Netherlands. *Cretaceous Research*, 24, 253–275.

Jeremiah, J.M., Duxbury, S. and Rawson, P. (2010) Lower Cretaceous of the southern North Sea Basins: reservoir distribution within a sequence stratigraphic framework. *Netherlands Journal of Geosciences*, 89, 203–237.

Kemper, E. (1973) Das Berrias (tiefe Unterkreide) in NW-Deutschland. *Geologisches Jahrbuch*, A9, 47–67.

Kemper, E. (1976) Geologischer Führer durch die Grafschaft Bentheim und die angrenzenden Gebiete mit einem Abriß der emländischen Unterkreide. In: Heimatverein der Grafschaft Bentheim (Ed.), *Das Bentheimer Land*. Nordhorn, Bentheim: Verlag Heimatverein der Grafschaft Bentheim e.V., pp. 1–206.

Kemper, E. (1979) Die Unterkreide Nordwestdeutschlands. In: Wiedmann, J. (Ed.), *Aspekte der Kreide Europas. International Union of Geological Sciences Series*, A6, 1–9.

Kemper, E. (1992) Die tiefe Unterkreide im Vechte-Dinkel-Gebiet: westliches niedersächsisches Becken. Stichting Het Staringmonument te Losser, 95 pp.

Kemper, E., Rawson, P. and Thieuloy, J.-P. (1981) Ammonites of Tethyan ancestry in the early Lower Cretaceous of north-west Europe. *Palaeontology*, 24, 251–311.

Kuhn, O., Weissert, H., Föllmi, K.B. and Hennig, S. (2005) Altered carbon cycling and trace-metal enrichment during the late Valanginian and early Hauterivian. *Eclogae Geologicae Helvetiae*, 98, 333–344.

Kujau, A., Nürnberg, D., Zielhofer, C., Bahr, A. and Röhl, U. (2010) Mississippi River discharge over the last ~560,000years – indications from X-ray fluorescence core-scanning. *Palaeogeography, Palaeoclimatology, Palaeoecology*, 298, 311–318.

Kylander, M.E., Ampel, L., Wohlfarth, B. and Veres, D. (2011) High-resolution X-ray fluorescence core scanning analysis of Les Echets (France) sedimentary sequence: new insights from chemical proxies. *Journal of Quaternary Science*, 26, 109–117.

Lazar, O.R., Bohacs, K.M., Macquaker, J.H.S., Schieber, J. and Demko, T.M. (2015) Capturing key attributes of fine-grained sedimentary rocks in outcrops, cores, and thin sections: nomenclature and description guidelines. *Journal of Sedimentary Research*, 85, 230–246.

Lini, A., Weissert, H. and Erba, E. (1992) The Valanginian carbon isotope event: a first episode of greenhouse climate conditions during the Cretaceous. *Terra Nova*, 4, 374–384.

Macquaker, J.H.S. and Taylor, K.G. (1996) A sequence-stratigraphic interpretation of a mudstone-dominated succession: the Lower Jurassic cleveland ironstone formation, UK. *Journal of the Geological Society*, 153, 759–770.

Macquaker, J.H.S., Gawthorpe, K.G., Taylor, K.G. and Oates, M.J. (1998) Hetrogeneity, stacking patterns and sequence stratigraphy in distal mudstone successions; examples from the Kimmeridge Clay Formation. In: Schieber, J., Zimmerle, W. and Sethi, P.S. (Eds.) *Shales and Mudstones; I, Basin Studies, Sedimentology, and Palaeontology*. Stuttgart: E. Schweizerbart'sche Verlagsbuchhandlung, pp. 163–186.

Macquaker, J.H.S., Taylor, K.G. and Gawthorpe, R.L. (2007) High-resolution facies analyses of mudstones: implications for Paleoenvironmental and sequence stratigraphic interpretations of offshore ancient mud-dominated successions. *Journal of Sedimentary Research*, 77, 324–339.

Macquaker, J.H.S., Keller, M.A. and Davies, S.J. (2010) Algal blooms and "Marine Snow": mechanisms that enhance preservation of organic carbon in ancient fine-grained sediments. *Journal of Sedimentary Research*, 80, 934–942.

Martin, G.P.R. (1961) Eine marine Mikrofauna im Wealden von Emlichheim (Emsland, NW-Deutschland). *Palaeontographica A*, 116, 105–121.

Martinez, M., Deconinck, J.-F., Pellenard, P., Riquier, L., Company, M., Reboulet, S. *et al*. (2015) Astrochronology of the Valanginian-Hauterivian stages (Early Cretaceous): chronological relationships between the Paraná-Etendeka large igneous province and the Weissert and the Faraoni events. *Global and Planetary Change*, 131, 158–173.

Matys Grygar, T., Hošek, M., Mach, K., Schnabl, P. and Martinez, M. (2017) Climatic instability before the Miocene climatic optimum reflected in a Central European lacustrine record from the most Basin in the Czech Republic. *Palaeogeography, Palaeoclimatology, Palaeoecology*, 485, 930–945.

Matys Grygar, T., Mach, K. and Martinez, M. (2019) Checklist for the use of potassium concentrations in siliciclastic sediments as paleoenvironmental archives. *Sedimentary Geology*, 382, 75–84.

Menegatti, A.P., Weissert, H., Brown, R.S., Tyson, R.V., Farrimond, P., Strasser, A. *et al*. (1998) High-resolution $\delta^{13}C$ stratigraphy through the Early Aptian "Livello selli" of the Alpine tethys. *Paleoceanography*, 13, 530–545.

Michael, E. (1974) Zur Paläoökologie und Faunenführung im westlichen Bereich des norddeutschen Unterkreide-Meeres. *Geologisches Jahrbuch*, A19, 1–68.

Michael, E. (1979) Mediterrane Fauneneinflüsse in den borealen Unterkreide-Becken Europas, besonders Nordwestdeutschlands. In: Wiedmann, J. (Ed.), *Aspekte der Kreide Europas. International Union of Geological Sciences Series*, A6, 305–321.

Möller, C. and Mutterlose, J. (2014) Middle Hauterivian biostratigraphy and palaeoceanography of the Lower Saxony Basin (Northwest Germany). *Zeitschrift der Deutschen Gesellschaft für Geowissenschaften*, 165, 501–520.

Monien, D., Kuhn, G., von Eynatten, H. and Talarico, F.M. (2012) Geochemical provenance analysis of fine-grained sediment revealing Late Miocene to recent Paleo-Environmental changes in the Western Ross Sea, Antarctica. *Global and Planetary Change*, 96–97, 41–58.

Muhs, D.R., Bettis Iii, E.A., Been, J. and McGeehin, J.P. (2001) Impact of climate and parent material on chemical weathering in loess-derived soils of the Mississippi River valley. *Soil Science Society of America Journal*, 65, 1761–1777.

Müller, H.-W., Dohrmann, R., Klosa, D., Rehder, S. and Eckelmann, W. (2009) Comparison of two procedures for particle-size analysis: Köhn pipette and X-ray granulometry. *Journal of Plant Nutrition and Soil Science*, 172, 172–179.

Mutterlose, J. (1992) Migration and evolution patterns of floras and faunas in marine Early Cretaceous sediments of NW Europe. *Palaeogeography, Palaeoclimatology, Palaeoecology*, 94, 261–282.

Mutterlose, J. and Böckel, B. (1998) The Barremian-Aptian interval in NW Germany: a review. *Cretaceous Research*, 19, 539–568.

Mutterlose, J. and Bornemann, A. (2000) Distribution and facies patterns of Lower Cretaceous sediments in northern Germany: a review. *Cretaceous Research*, 21, 733–759.

Mutterlose, J. and Ruffell, A. (1999) Milankovitch-scale palaeoclimate changes in pale–dark bedding rhythms from the Early Cretaceous (Hauterivian and Barremian) of eastern England and northern Germany. *Palaeogeography, Palaeoclimatology, Palaeoecology*, 154, 133–160.

Mutterlose, J. and Wiedenroth, K. (2009) Neue Tagesaufschlüsse der Unter-Kreide (Hauterive – Unter-Apt) im Großraum Hannover – Braunschweig: stratigraphie und Faunenführung. *Berliner Paläobiolog Abh*, 10, 257–288.

Mutterlose, J., Wippich, M.G.E. and Geisen, M. (1997) Cretaceous depositional environments of NW Germany. *Bochumer Geologische und Geotechnische Arbeiten*, 46, 1–134.

Mutterlose, J., Pauly, S. and Steuber, T. (2009) Temperature controlled deposition of early Cretaceous (Barremian–early Aptian) black shales in an epicontinental sea. *Palaeogeography, Palaeoclimatology, Palaeoecology*, 273, 330–345.

Pauly, S., Mutterlose, J. and Wray, D.S. (2013) Palaeoceanography of Lower Cretaceous (Barremian–Lower Aptian) black shales from northwest Germany evidenced by calcareous nannofossils and geochemistry. *Cretaceous Research*, 42, 28–43.

Peksa, A.E., Wolf, K.-H.A.A. and Zitha, P.L.J. (2015) Bentheimer sandstone revisited for experimental purposes. *Marine and Petroleum Geology*, 67, 701–719.

Picard, M.D. (1971) Classification of fine-grained sedimentary rocks. *Journal of Sedimentary Research*, 41, 179–195.

Piva, A., Asioli, A., Schneider, R.R., Trincardi, F., Andersen, N., Colmenero-Hidalgo, E. *et al*. (2008) Climatic cycles as expressed in sediments of the PROMESS1 borehole PRAD1-2, central Adriatic, for the last 370 ka: 1. Integrated stratigraphy. *Geochemistry, Geophysics, Geosystems*, 9, Q01R01, https://doi.org/10.1029/2007GC001713.

Rawson, P. and Riley, L.A. (1982) Latest Jurassic-Early Cretaceous events and the "late Cimmerian unconformity" in North Sea area. *AAPG Bulletin*, *66*, 2628–2648.

Rothwell, R.G. and Rack, F.R. (2006) New techniques in sediment core analysis: an introduction. *Geological Society of London Special Publications*, *267*, 1–29.

Rowe, H., Wang, X., Fan, B., Zhang, T., Ruppel, S.C., Milliken, K.L. *et al.* (2017) Chemostratigraphic insights into fluvio-lacustrine deposition, Yanchang Formation, Upper Triassic, Ordos Basin, China. *Interpretation*, *5*, SF149–SF165.

Ruffell, A. (1991) Sea-level events during the Early Cretaceous in Western Europe. *Cretaceous Research*, *12*, 527–551.

Salabarnada, A., Escutia, C., Röhl, U., Nelson, C.H., McKay, R., Jiménez-Espejo, F.J. *et al.* (2018) Paleoceanography and ice sheet variability offshore Wilkes Land, Antarctica – Part 1: insights from late Oligocene astronomically paced contourite sedimentation. *Climate of the Past*, *14*, 991–1014.

Sano, J.L., Ratcliffe, K.T. and Spain, D.R. (2013) Chemostratigraphy of the Haynesville Shale. *AAPG Bulletin*, *105*, 137–154.

Schieber, J. (1996) Early diagenetic silica deposition in algal cysts and spores; a source of sand in black shales? *Journal of Sedimentary Research*, *66*, 175–183.

Schieber, J. and Baird, G. (2001) On the origin and significance of pyrite spheres in Devonian Black shales of North America. *Journal of Sedimentary Research*, *71*, 155–166.

Schieber, J., Krinsley, D. and Riciputi, L. (2000) Diagenetic origin of quartz silt in mudstones and implications for silica cycling. *Nature*, *406*, 981–985.

Schneider, A.C., Heimhofer, U., Heunisch, C. and Mutterlose, J. (2018) The Jurassic-Cretaceous boundary interval in non-marine strata of northwest Europe – new light on an old problem. *Cretaceous Research*, *87*, 42–54.

Schott, W., Jaritz, W., Kockel, F., Sames, C.W., Stackelberg, V., Stets, J. *et al.* (1967/1969) *Paläogeographischer Atlas der Unterkreide von Nordwestdeutschland mit einer Übersichtsdarstellung des nördlichen Mitteleuropa*. Hannover: Bundesanst. f. Bodenforsch.

Schwalbach, J.R., Bohacs, K.M., White, L.D. (1992) *Sequence stratigraphy in fine-grained rocks: examples from the Monterey Formation*. Pacific Section, SEPM. Bakersfield: Society for Sedimentary Geology, 80 pp.

Singh, P. (2008) Lithofacies and sequence stratigraphic framework of the Barnett Shale, Northeast Texas, Univ. Oklahoma, PhD thesis, 199 pp.

Stadtler, A. (1998) Der Bentheimer Sandstein (Valangin, NW-Deutschland): eine palökologische und sequenzstratigraphische Analyse. *Bochumer Geologische Und Geotechnische Arbeiten*, *49*, 1–127.

Stow, D.A.V. (1981) Fine-grained sediments: terminology. *Quarterly Journal of Engineering Geology Hydrogeology*, *14*, 243–244.

Tjallingii, R. (2007) *Application and quality of X-ray fluorescence core scanning in reconstructing Late Pleistocene NW African continental margin sedimentation patterns and paleoclimate variations*, PhD thesis. University of Bremen, 114 pp.

Turner, B.W., Molinares-Blanco, C.E. and Slatt, R.M. (2015) Chemostratigraphic, palynostratigraphic, and sequence stratigraphic analysis of the Woodford Shale, Wyche Farm Quarry, Pontotoc County, Oklahoma. *Interpretation*, *3*, SH1-SH9, https://doi.org/10.1190/INT-2014-0089.1.

Turner, B.W., Tréanton, J.A. and Slatt, R.M. (2016) The use of chemostratigraphy to refine ambiguous sequence stratigraphic correlations in marine mudrocks. An example from the Woodford Shale, Oklahoma, USA. *Journal of the Geological Society*, *173*, 854–868.

Ver Straeten, C.A., Brett, C.E. and Sageman, B.B. (2011) Mudrock sequence stratigraphy: a multi-proxy (sedimentological, paleobiological and geochemical) approach, Devonian Appalachian Basin. *Palaeogeography, Palaeoclimatology, Palaeoecology*, *304*, 54–73.

Wang, M., Zheng, H., Xie, X., Fan, D., Yang, S., Zhao, Q. *et al.* (2011) A 600-year flood history in the Yangtze River drainage: comparison between a subaqueous delta and historical records. *Chinese Science Bulletin*, *56*, 188–195.

Wedepohl, K.H. (1971) Environmental influences on the chemical composition of shales and clays. *Physics and Chemistry of the Earth*, *8*, 307–333.

Weissert, H. (1990) Siliciclastics in the early Cretaceous Tethys and North Atlantic oceans: documents of periodic greenhouse climate conditions. *Memorie Società Geologica ltaliana*, *44*, 59–69.

Weissert, H., Lini, A., Föllmi, K.B. and Kuhn, O. (1998) Correlation of Early Cretaceous carbon isotope stratigraphy and platform drowning events: a possible link? *Palaeogeography, Palaeoclimatology, Palaeoecology*, *137*, 189–203.

Weltje, G.J. and Tjallingii, R. (2008) Calibration of XRF core scanners for quantitative geochemical logging of sediment cores: theory and application. *Earth and Planetary Science Letters*, *274*, 423–438.

Weltje, G.J. and von Eynatten, H. (2004) Quantitative provenance analysis of sediments: review and outlook. *Sedimentary Geology*, *171*, 1–11.

Westermann, S., Föllmi, K.B., Adatte, T., Matera, V., Schnyder, J., Fleitmann, D. *et al.* (2010) The Valanginian δ^{13}C excursion may not be an expression of a global oceanic anoxic event. *Earth and Planetary Science Letters*, *290*, 118–131.

Wolburg, J. (1959) Die Cyprideen des NW-deutschen Wealden. *Senckenbergiana Lethaea*, *40*, 223–315.

Wonham, J., Johnson, H., Mutterlose, J., Stadtler, A. and Ruffell, A. (1997) Characterization of a shallow marine sandstone reservoir in a syn-rift setting: the Bentheim Sandstone Formation (Valanginian) of the Rühlermoor field, Lower Saxony Basin, NW Germany. In: Shallow marine and nonmarine reservoirs, sequence stratigraphy, reservoir architecture, and production characteristics, 18th Annual Research Conference, Gulf Coast Association of Geological Societies, pp. 427–448.

Wortmann, U.G. and Weissert, H. (2000) Tying platform drowning to perturbations of the global carbon cycle with δ^{13}C$_{Org}$-curve from the Valanginian of DSDP Site 416. *Terra Nova*, *12*, 289–294.